Contextualising archaeological models with geological, airborne and terrestrial LiDAR data: the Ice Age landscape in Farndon Fields, Nottinghamshire, UK

DEODATO TAPETE [a, *], VANESSA BANKS [a], LEE JONES [a], MATTHEW KIRKHAM [a], DARYL GARTON [b]

[a] British Geological Survey, Natural Environment Research Council, Nicker Hill, Keyworth, NG12 5GG, UK;

[b] Beeston, Nottinghamshire

[*] Corresponding author. Telephone: +44 (0) 115 936 3537
E-mail address: deodato@bgs.ac.uk; deodato.tapete@gmail.com

ABSTRACT

Archaeological models of past human occupation of the landscape build upon the understanding of the natural palaeo-environment. This cognitive process relies on the study of the sediment units at a level of spatial resolution that might not be achieved with available maps. This paper presents a new approach to combine traditional ground investigation methods and new technologies to detect, extract and analyse stratigraphic records, with particular application to vanishing landscapes with limited exposure of the sediments. The demonstration site is Farndon Fields, an extremely rare Late Upper Palaeolithic open-air site at the southern outskirts of Newark-on-Trent in Nottinghamshire, UK. Since the early 1990s when the upgrading of the new A46 road was planned, ground and archaeological investigations have been carried out. The test-pitting undertaken by Farndon Archaeological Research Investigations (FARI) in the field 373A in September 2015 offered an ideal occasion for the British Geological Survey (BGS) to test the methodology. A palaeo-geographic understanding from regional to local scales is here proposed based on 5-m airborne Light Detection and Ranging (LiDAR) data and multispectral aerial photographs of the site prior to the alteration due to the A46 works. Features of the palaeo-landscape are vanishing and intrusive investigations are required to unveil the presence of the archaeological context. Samples were taken for particle size analysis of the sediment units to characterise the aeolian sand deposits ('coversands') and the underlying clayey silty sandy sediments interbedded with paler laminae. For the first time state-of-the-art terrestrial LiDAR technology was

used for stratigraphic profiling, strata delineation and geological feature extraction based on the intensity return and surface roughness. The combined use of point clouds, 3D models and cloud intensity from terrestrial LiDAR provides an added level of confidence to the ability to subdivide the sediment units and discriminate them from ploughsoil. Internal bedding of the coversands is enhanced in the LiDAR elaborations. This is new evidence not otherwise observed by the naked eye. On the other side, the classification of point clouds by roughness index seems promising for recording the grading of the sediments. The experiment in Farndon Fields therefore demonstrates the benefit of phased technology-based investigation combining archaeology and geology towards a more cost-effective assessment through strategic sampling and digital recording of landscape domains.

KEYWORDS

Anthropogenic deposits; palaeo-environment; coversands; geological mapping; LiDAR; terrestrial laser scanner; Farndon Fields

1 INTRODUCTION

'Geoarchaeology' is an established sub-discipline of archaeology which promotes the application of earth-science approaches to archaeological interpretation (Rapp and Hill, 2006) to study soils, palaeosoils, anthrosoils and sediment units of archaeological sites and cultural landscapes. Test-pits and trench excavation are the traditional intrusive methods used to corroborate hypotheses of archaeological potential, understand the processes that formed and protected an archaeological site (Schiffer, 1987) and investigate palimpsests (Bailey, 2007).

However, discrimination of archaeological horizons from and throughout geological strata is still a challenging task (see Edgeworth et al., 2015 for the recent debate in the Anthropocene research field). Through time sediment units may have been altered by biological processes, roots and ploughing. Once exposed to open air, they also may oxidise or be washed out if not properly sheltered during the archaeological survey. Even in good visibility conditions, cost-effective means for objective documentation are required to: record the exposed features more quickly; allow digital accessibility to the stratigraphy when test-pits and trenches are closed; collect spatial information over wide surfaces; optimise the selection of the points from which samples are taken and then investigated in the lab.

Emerging technologies of geological mapping and documentation, such as Light Detection and Ranging (LiDAR), are therefore helpful and allow digital storage of information. Recent literature (Challis, 2005; 2006; Malone, 2012) demonstrate that LiDAR data taken from aircrafts can be valuable for discoveries of geoarchaeological resources in alluvial environments. Nevertheless, limits can be found at the landscape scale for the identification of spatial patterns and discrimination of differential preservation potential (Challis et al., 2011).

At another scale, techniques for digital data capture using ground-based instrumentation – namely close-range photogrammetry, terrestrial laser or structured light scanners – can be more suitable for archaeological fieldwork. Lerma et al. (2014) recorded exposed surfaces and manmade artefacts; Sanger (2005) analysed depositional events; Doneus and Neubauer (2005, 2006) documented temporary layers and units of stratification during the progress of stratigraphic excavations; Fisher et

al. (2015) created a full digital record of the archaeological survey and visualised results of laboratory analyses in the correct sampling locations along the stratigraphic columns. These examples prove that digital technologies are increasingly integrated in the cognitive and analytical process of archaeological excavations.

In this context, our paper aims to explore the process by which LiDAR data taken with airborne and terrestrial instrumentation can support a geoarchaeological study to upscale regional geological data, complement profiling of archaeological stratigraphy and characterise sediment units.

We provide a demonstration through the results obtained in the Late Upper Palaeolithic (LUP) open-air site at Farndon Fields, Nottinghamshire (UK). This is a nationally important site which may preserve the most significant geoarchaeological resource in the country referring to the intermittent re-visits of the hunter community that first colonised Britain after the Last Glacial Maximum (Jacobi and Higham, 2009; English Heritage, 2012; Highways Agency, 2012).

Section 2 provides an introduction to Farndon Fields, its geological setting and archaeological resources. Section 3 describes the methodological approach of in-situ ground investigations and laboratory analyses. Section 4 presents the research outcomes in a multi-scale perspective, from regional to local scales. Section 5 outlines the significance of the geological evidence collected in September 2015 through LiDAR to frame and contextualise the archaeological model of human occupation of Farndon in LUP. Section 6 summarises the long-term benefits of digital recording of temporary excavations and outlines future directions of research.

2 FARNDON FIELDS

'Farndon Fields' is the toponym of our study area located in the flattish interfluve on the Holme Pierrepont Terrace of the River Trent (centre coordinates: WGS84 53.059229° N; 0.839340° W; OS Grid Reference SK 77883 51960; 477883.776,351960.501), less than 2 km south-west of where the tributary River Devon joins the River Trent at Newark (Figure 1). The site is presently privately-

owned cropland and, with permission, can be accessed from Fosse Way. This road passes through the modern village of Farndon following the former course of the namesake Roman road.

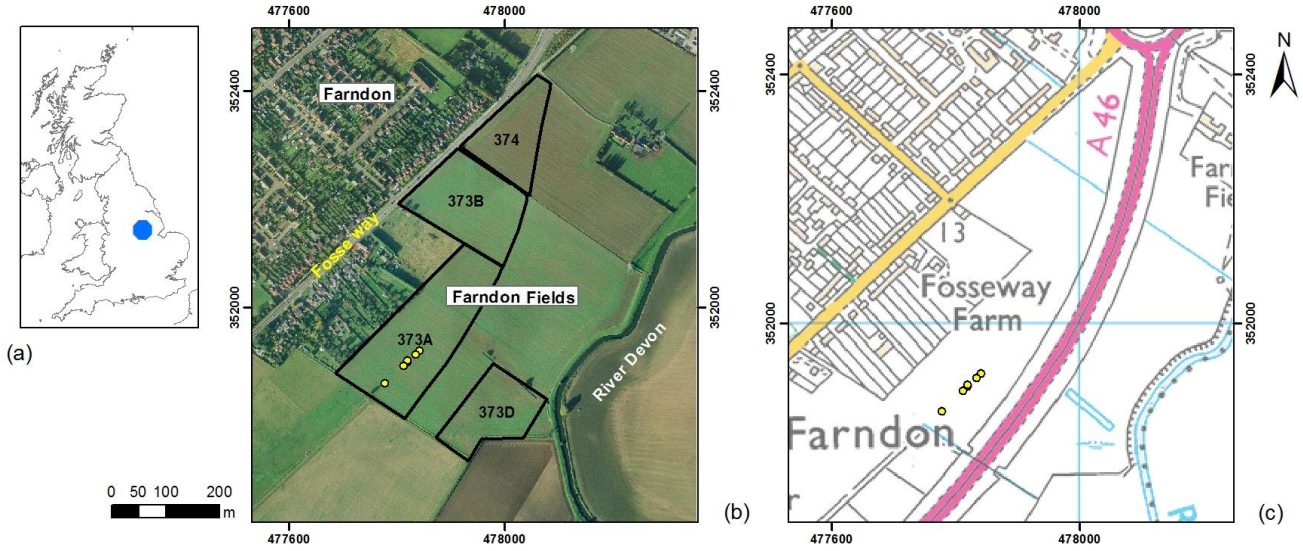

Figure 1 – Farndon Fields, south of Newark-on-Trent, Nottinghamshire, England, UK: (a) location map; (b) aerial view of the site prior to the construction of A46 road, with indications of the fields surveyed by Farndon Archaeological Research Investigations (FARI); (c) Ordnance Survey (OS) topographic map at 1:25,000 scale including the route of the A46 and the Farndon roundabout. Yellow dots in (b) and (c) indicate the station points from which the test-pits (TP) dug out by FARI during the archaeological survey in 2015 were scanned by the British Geological Survey (BGS) with terrestrial laser scanner (TLS). British National Grid; Projection: Transverse Mercator; Datum: Ordnance Survey Great Britain (OSGB) 1936. Contains OS data © Crown Copyright and database rights 2016. Aerial photography © UKP/Getmapping Licence No. UKP2006/01.

2.1 Geological setting

The geological setting is summarised in Table 1 and displayed in the geological maps of the superficial deposits and bedrock geology in Figure 2. The geological information come from: the Mineral Assessment Report by Price and Rogers (1978); mineral assessment surveys undertaken by the Institute of Geological Sciences (now the British Geological Survey – BGS) during the 1970s and 1930s; the current 1:50,000 scale map (E126; BGS, 1996); the digital equivalent at 1:50,000 and 1:10,000 scales (BGS, 2016a); and the sheet memoir (Howard et al., 2009). The geological terminology used in Figure 2 and in this paragraph follows the BGS Lexicon of Named Rock Units

(BGS, 2017). The recent geological research on the terraces of the River Trent (Bridgland et al., 2014) has been taken into account.

The site is underlain by bedrock comprising the Edwalton Member of the Sidmouth Mudstone Formation. This is capped by the Holme Pierrepont Sand and Gravel Member of the Trent Valley Formation. The Balderton Sand and Gravel Member (Brandon and Sumbler, 1991) caps the higher terrace to the east and ribbons of Alluvium occupy the flood plains of the Rivers Trent and Devon. Holocene and Devensian Head deposits, including colluvium, are particularly associated with the edges of the terraces. The 1:10,000 mapping recorded on the field slip indicates that the surface expression of the Holocene Alluvium evident in the area of field 373D (i.e. in the field located south-east of the area investigated in 2015; Figure 1b) comprises “brown and ochre clays” at surface, whilst the Holme Pierrepont Member is characterised by “brown loamy sand with abundant gravel (of Bunter and flint)”. The term “Bunter” is a reference to pebbles that are derived from the Sherwood Sandstone Group that outcrops in the order of 14 km to the west of Farndon. These are well rounded pebbles, predominantly of quartzite. Logging of ditch sections indicates that the near surface strata were underlain by gravels at about 1.7 m depth. The superficial deposits named “Head” blanket the gentle slopes on the inside of the meander on the eastern side of the River Devon (Figure 2a).

Further to the BGS mapping more detailed environmental analysis of the Holme Pierrepont Sand and Gravel Member has been undertaken through the Aggregates Levy Sustainability Fund (Howard et al., 2011). This research confirmed the cool climatic conditions of deposition of the Holme Pierrepont terrace deposits, suggesting that it was laid down in two pulses, immediately prior to and post the Loch Lomond stadial (Younger Dryas Marine Isotope Stage (MIS) 1).

127 **Table 1 –** Geological succession of Farndon Fields, Nottinghamshire (lithology based on Howard et al., 2009).

Group/ Subgroup	**Formation**	**Member**	**Lithology**
Trent-Witham Catchment	Trent Valley	Hemington	Holocene Alluvium associated with the modern rivers (Trent and Devon).
		Holme Pierrepont	Late Devensian, predominantly cold-phase sands and gravels that underlie the Holme Pierrepont Terrace. The Holme Pierrepont Sand and Gravel Member includes the Spalford Sand (type area: Spalford [SK 840 690], Nottinghamshire). The Spalford Sand comprises spreads of pale brown, fine grained blown sand, up to about 3 m thick, overlying the sand and gravel. It is thought to be Late Devensian (MIS 2), possibly Late Glacial in age (Brandon and Sumbler, 1988).
		Balderton Sand and Gravel (Older Gravel)	Predominantly cold phase sands and gravels that underlie the Balderton Terrace; includes aeolian coversands and periglacial deposits.
Penarth	Sidmouth Mudstone Formation	Edwalton Member	Red-brown and greenish grey Triassic mudstones and siltstones, with beds of siltstone and very fine-grained sandstone common in the lower half; finely disseminated gypsum common in upper half.
		Cotgrave Member	Triassic pale greenish grey fine- to medium-grained sandstone, interbedded with dark greenish-grey mudstone and siltstone. Gypsum nodules occur throughout.
		Gunthorpe Member	Red-brown mudstone, with subordinate greenish grey siltstone and fine-grained sandstone and common gypsum veins and nodules.

128

129

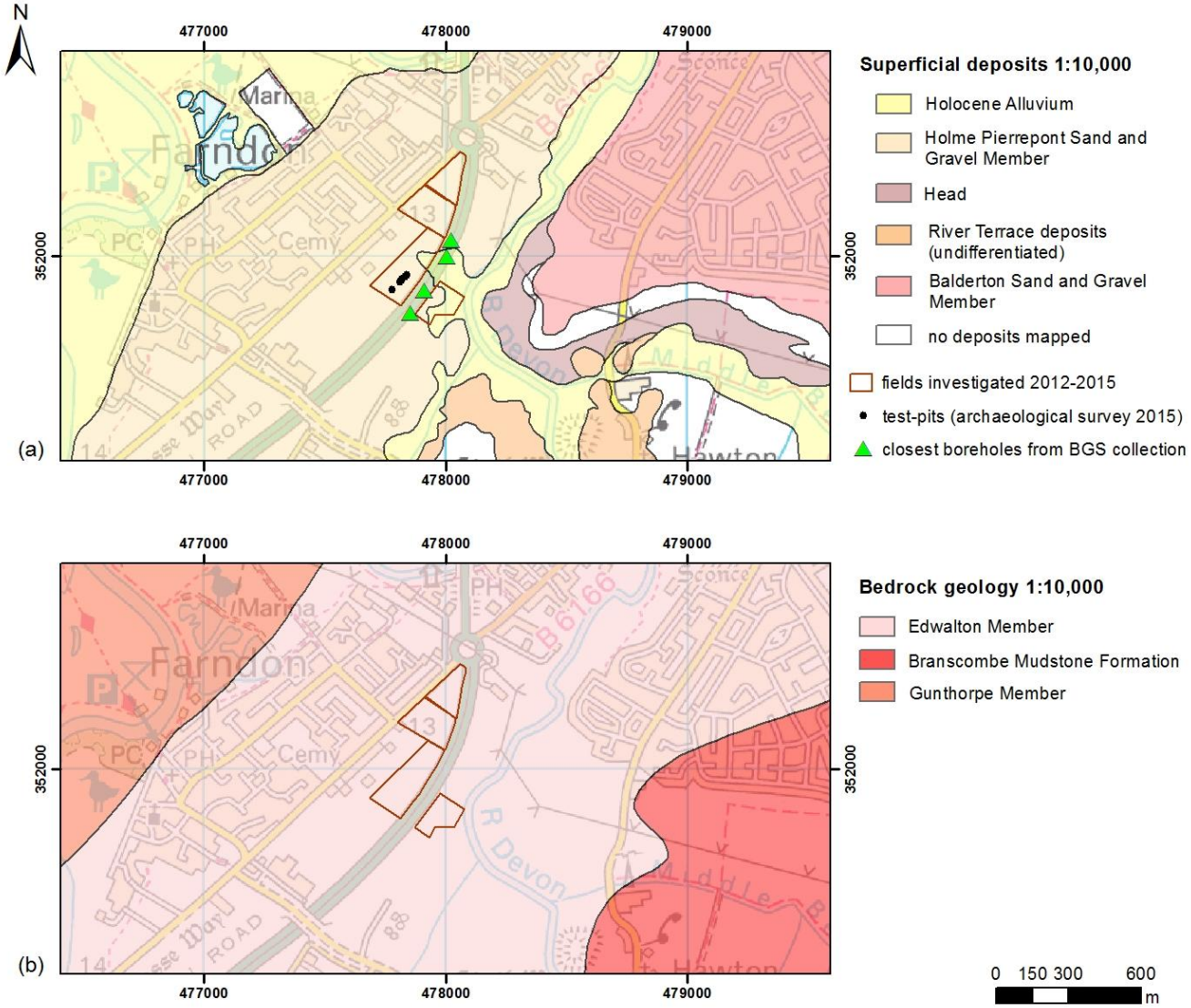

130

131 **Figure 2 –** Geological maps of (a) superficial deposits and (b) bedrock geology based on BGS' Digital
132 Geological Map of Great Britain (DiGMapGB) at 1:10,000 scale (BGS, 2016a), with location of the boreholes
133 closest to the field 373A (see also Figure 1 and Figure 3) that were drilled for the A46 Newark to Widmerpool
134 improvements and can be consulted via BGS' Geology of Britain Viewer (BGS, 2016b). British National Grid;
135 Projection: Transverse Mercator; Datum: OSGB 1936. Geological materials © Natural Environment Research
136 Council (NERC). All rights reserved 2016. Contains OS data © Crown Copyright and database rights 2016.

137

138

139

140

2.2 Archaeological resources

The archaeological potential of alluvial deposits and geomorphological settings across the Trent Valley has been investigated and modelled by Brown et al. (2005, 2007) and Howard et al. (2008). This research proved how river confluence zones and their adjacent floodplains could be ideal sites for hunter communities. In particular, by incorporating within the GIS archaeological records, BGS geological data at 1:50,000 mapping scale and airborne LiDAR, Howard et al. (2008) found that at the confluence zone of the Rivers Trent and Soar, north of Kegworth, the Holme Pierrepont Sand and Gravel "represents a stable land surface of considerable antiquity and offers the potential to preserve multi-period archaeological remains (i.e. Upper Palaeolithic to post-medieval)".

The archaeological importance of Farndon Fields was proved in 1991, when the proposed construction of the new A46 road – which currently runs diagonally across the site (Figure 1c) – was initiated by the Highways Agency. This infrastructure work triggered the planning context for a series of systematic fieldwalking campaigns and site investigations (Garton, 1993; Garton and Jacobi, 2009; Highways Agency, 2012; Kinsley and Knight, 1992; Wessex Archaeology, 1995; and for a review of past and recent fieldwork in Farndon see Garton et al., 2015). This research allowed the discovery of significant in-situ concentrations of flintwork and microdebitage attributed to two distinctive Creswellian and Federmesser LUP blade technologies (c. 14,700 to c. 12,900 cal BP; Highways Agency, 2012; Harding et al., 2014). The findings stimulated the speculation whether these flint scatters might testify that Farndon Fields was a temporary settlement of hunter-gatherer bands ranging between the Trent Valley and the cave sites of the Magnesian Limestone escarpment (Knight, 2004; Knight et al., 2012) and seeking the fresh water available at this site (Highways Agency, 2012). Farndon Fields was further investigated since 2012 by the voluntary group 'Ice Age Journeys', with the aim to determine the state of preservation of the sediment units outside the road-line. Both northern (ID 374, 373B) and southern (ID 373A, 373D) fields (Figure 1b) were studied using a combination of fieldwalking, augering and test-pitting. The findings have been recently presented and discussed by Garton et al. (2015).

A key discovery of this report is the evidence that previously undisturbed LUP clusters and scatters have begun to be severely damaged by recent ploughing. This process has been observed in particular in the southern fields, in locations that are close to relatively thick alluvium and wind-blown sand deposits (called 'coversand'), where Garton et al. (2015) hypothesised that more complete Late Glacial sequences might be better preserved.

It is worth recalling that the East Midlands are also one of the few regions in Britain where there is evidence of Late Pleistocene 'coversands'. This term indicates periglacial, aeolian sand deposits consisting of moderate to well-rounded spherical, well-sorted sand particles (mean grain size of about 150-200 μm), lacking interstitial silt and clay, with a low percentage of the fraction finer than 63 μm. Layering is largely horizontal or sub-horizontal (Baker et al., 2013). Generally, coversands manifest as a relatively flat and thin mantle (<5 m) over older sediments, extending from a few to thousands of square kilometres (Bateman, 1995, 1998). Contrasting with the European geological stratigraphies, British coversand deposits tend to be limited in extent and fragmented (Baker et al., 2013). Dating evidence suggests that a number of periods of deposition are represented in Britain. In Lincolnshire, thermoluminescence dating by Bateman (1995) suggests contemporaneity with the Younger Coversand II in the European coversand chronology (Koster, 1988). There remains uncertainty about the processes of coversand deposition, local fluvial and niveo-aeolian deposition and reworking may have supplemented the initial wind transportation of sediments derived from open and bare surfaces during cold periods (Bateman, 1995 and references therein; Garton et al., 2015).

Baker et al. (2013) reviewed the records of 'coversands' in the Trent valley as an indicator of environmental change during the Late Pleistocene and early Holocene. Coversands at Farndon occur as outliers of limited extent, filling palaeo-hollows in the valley floodplain. They are the most southerly remnants of a coversand sheet extending into this eastern region of Great Britain. Lower Trent coversands formally belong to the Spalford Sand Member of the Trent Valley Formation (Brandon and Sumbler, 1988), the depositional environment of which is described in Baker et al. (2013) and Howard et al. (2007).

An additional layer of data has come from the trial pits excavated for the A46 road improvement scheme, comprising archaeological resource and mitigation (associated with the geotechnical survey of the proposed route) investigations (Wessex Archaeology, 1995, 2006). This work provided more detail on the near surface soils distinguished into (Wessex Archaeology, 2006):

- "the topsoil (ploughsoil) typically comprised dark greyish brown [...] non-calcareous heavy clay loam, and generally 0.3-0.35 m across the Site [Farndon Fields]";
- "the subsoil, varying in thickness between 0.2 m and 0.9 m, was recorded in all trial pits [...] either very sandy clay or clayey sand of variable colours, although generally yellowish brown".

The upper levels of the "subsoil" were noted to have been disturbed by bioturbation and cryoturbation processes. According to Harding et al. (2014), "variations in the subsoil (including several clearly defined units)" could be taken as "indicative of episodic pre-Holocene alluviation and/or solifluction, which could have preserved surfaces and/or horizons containing LUP material below the present ploughsoil (TPAU, 2004)".

Whilst the association of the Late Upper Palaeolithic activity (14,700 to 12,900 BP) with the Holme Pierrepont Terrace in Farndon was established through fieldwalking (Garton, 1993; Wessex Archaeology, 1995, 2006; Knight and Howard, 2004), the subsequent intrusive archaeological investigations identified: (i) the difficulty that there has been in establishing in-situ subsurface buried landscape of occupation terraces; (ii) the in-situ nature of the archaeological finds, largely unaffected by the periglacial activity evident in the in-situ strata, and (iii) the impact of the plough depth on the archaeological resource (Harding et al., 2014; Garton et al., 2015).

All the above highlights the archaeological importance of these wind-blown and fluvial sediment units, as well as the challenge faced by archaeologists in Farndon to establish a method for their interpretation as clearly defined units. These sediment units were therefore the subject of the laboratory analyses (sections 3.2 and 4.3) and LiDAR experiment (sections 3.4 and 4.4) of this research.

3 MATERIALS AND METHODS

3.1 Test-pitting

Figure 3a shows a zoomed aerial view of Farndon Fields, with the location of the archaeological cross-section A-A' investigated by Farndon Archaeological Research Investigations (FARI) in September 2015 by test-pitting the Field 373A. This area of Farndon Fields is located south of the excavations made by FARI in 2014 and had been investigated in 2013 by systematic fieldwalking, where the distribution of artefacts on the surface of the ploughed field had been recorded (Garton et al., 2015), and by a dedicated hand-augering survey using a dutch-head in January 2015 (unpublished report for Ice Age Journeys by William G. Mills, PhD student at the University of Oxford). This augering identified a sand deposit, provisionally interpreted as coversands, thickest in the area where fieldwalking had not located LUP artefacts. Nick Barton (University of Oxford) had raised the possibility that coversands might have buried LUP activity and artefacts might still lie below the reach of modern agriculture, so they would not be found by fieldwalking the ploughed field-surface. Hence a series of test-pits (TP) was located to sample the deepest sediment units and across the feather-edge of the potential coversand as it thinned to the north.

TP were opened by hand (using trowels, small hand-mattocks and spades) in spits (maximum depth 0.10 m) and a nominal size of 1 x 1 m to reach the sediment units at the bottom and expose the stratigraphic sequence. Western or northern inner pit-sections were documented and OS coordinates were taken at the ground level and key stratigraphic horizons.

To refer to the sediment units observed in the TP, hereinafter we use the following terms, from top to bottom: ploughsoil, coversands, fluvial deposits, gravel terrace. When the fluvial deposits are distinctively interbebbed with laminae, they are referred to as "laminated sediments" (see also section 4.2).

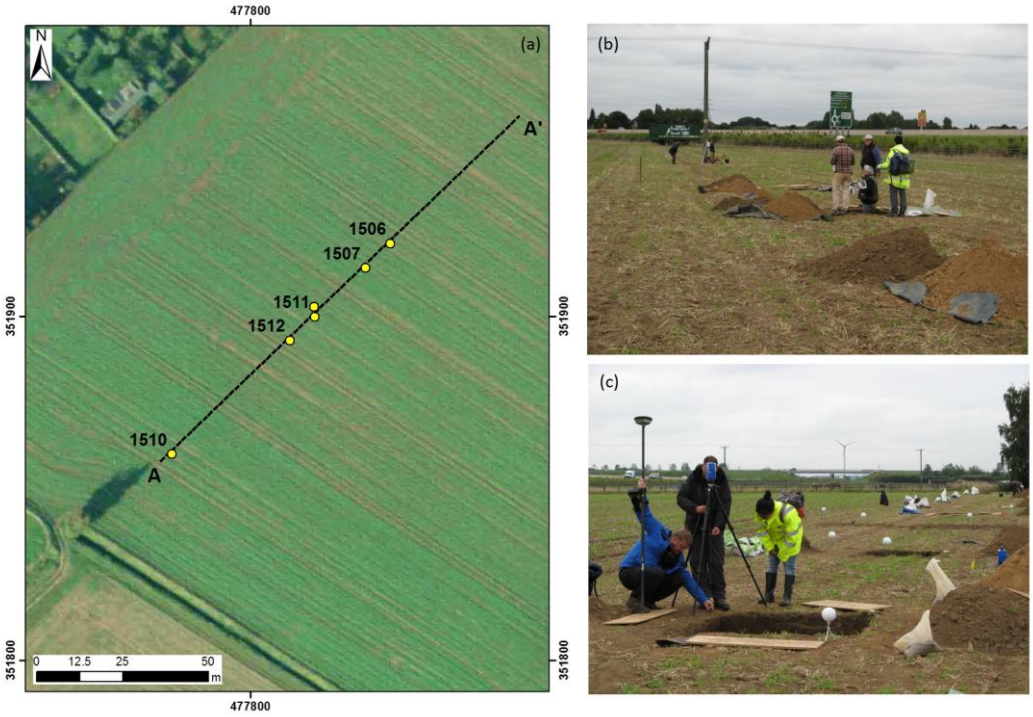

Figure 3 – Zoomed view of Farndon Fields, with location of: the archaeological cross-section A-A' investigated during the test-pitting undertaken in September 2015; and the terrestrial laser scanner stations (yellow dots) from which five of the test-pits (TP1510, 1512, 1511, 1507, 1506) were scanned. (© NERC. All rights reserved) (b) View of the TP and the proximity to the A46 road. (c) Terrestrial laser scanning acquisition of one of the TP (photo credit: Daryl Garton). British National Grid; Projection: Transverse Mercator; Datum: OSGB 1936. Aerial photography © UKP/Getmapping Licence No. UKP2006/01.

3.2 Sediment sampling and Particle Size Analysis (PSA)

Table 2 shows the list of bulk sediment samples that were collected through the stratigraphy within the TP. Location of the five TP is showed in Figure 3a. Particular attention was given to sample within the selected sediment units, avoiding the ploughsoil. The samples were then stored within water-proofed and sealed bags to preserve the moisture content.

Table 2 – Sediment samples collected from the TP in Farndon Fields during the archaeological survey in 2015 (for TP location and sample stratigraphic position see Figure 3a and Figure 6, respectively). Depth is measured from the ground surface; OS elevations are provided.

Test-pit	Section	Sample	Depth [cm]	OS elevation [m OD]	Description
1512	Western	1	94-101	11.32-11.39	Fluvial material only, below coversand and lying above the gravel terrace
	Western	2	85-92	top at 11.47	Transition to the coversand
	Western	3	75-82	11.51-11.58	Coversand
	Western	4	65-73	11.63	Coversand
	Western	5	53 - 63	11.46-11.56	Coversand
1510	Western	6	83 - 90	11.56-11.63	Fluvial material only, below coversand and lying above the gravel terrace
	Western	7	74 - 81	11.65-11.72	Transition to the coversand
	Western	8	64 - 71	11.75-11.82	Coversand
	Western	9	54 -61	11.85-11.92	Coversand
1511	Northern	10	93 - 102	11.27	Fluvial deposits, thicker upper reddish portion
1507	Western	11	83 - 94	11.09-11.20	Coversand (?)

Samples were taken from the western cross-sections of the TP, except for sample #10 from the northern face of TP1511. In TP1510 and 1512 the sediments were sampled sequentially, with a regular spacing (every 10 cm) moving up along the stratigraphy from the bottom fluvial sediments to the top coversands. Based on the field evidence (see section 4.2), we decided to recover two parallel sets of sediment samples, so we could achieve a good representation of the whole thickness of the coversands, including the transition with the underlying fluvial sediments. This type of sampling was meant to

highlight potential differences in grain size distribution by means of Particle Size Analysis (PSA). This choice was justified in light of two considerations. The coversands are likely to be the result of a sequence of depositional phases, associated to different environmental and energy conditions. Furthermore, given the relative stratigraphic position of TP1510 and TP1512 (see Figure 6), a parallel sediment sampling could provide evidence of stratigraphic correlations between these two TP, thereby helping to understand the overall stratigraphic and geological profiles (see section 4.2).

PSA were carried out using a combination of wet sieving technique for the coarser fraction (> 63µm) of the samples, and X-Ray Sedigraph for the finer fraction. Wet sieving was run according to the British Standards Institution (BSI) procedure described in BS 1377:1975, Test 7(A). The sieve spacing used to analyse the coarse fraction retained on the 0.063 mm sieve was 1Φ to 8.0 mm (-3 Φ) and then as required for larger particles. The total dry mass and each individual size fraction of each Particle Size Distribution (PSD) are weight to 0.01 g giving an overall error of around 0.1% for the PSD of the samples received. For the X-Ray Sedigraph analysis of the fine fraction, 5 g, oven dried, sub-sample was selected from the < 63µm washings of the whole sample and mixed with a 0.05% solution of sodium hexametaphosphate to form a suspension. The suspension was analysed in the X-ray Sedigraph, the results of which were then integrated with the coarse analysis. The X-ray Sedigraph system was calibrated with a garnet standard of known particle size distribution prior to testing to ensure accuracy of the results.

3.3 Airborne LiDAR and Radar

The topography of Farndon Fields is generally flat with gentle slopes towards the River Devon in the east, with slight hummocks and hollows having a maximum fall of some 1.2 m. Garton et al. (2015) has recently presented the elaboration by Ian Ross of LiDAR data licensed from the Environment Agency, to highlight ground levels between 10.5 and 12.0 m OD. The present paper extends this analysis using NEXTMap® Britain Digital Terrain Model (DTM) up to 5-m resolution (NEXTMap® Britain © 2003, Intermap Technologies Inc., All rights reserved), alongside true-colour Red-Green-Blue (RGB) and Infrared (IR) aerial photographs taken in May 2007 (tiles SK7751, SK7752, SK7851

294 and SK7852) and licensed to the BGS. These remote sensing datasets were useful to observe the
295 condition of Farndon Fields prior to the alteration due to the construction of the A46. We also used
296 these data to detect features of potential archaeological and palaeo-environmental interest, also in
297 relation to what was known from the fieldnotes and memoirs available at the BGS and already recalled
298 in section 2.1.

299 ### *3.4 Terrestrial LiDAR scanning (TLS) survey and texture extraction*

300 To upscale the geological mapping in Farndon Fields and record the exposed geology, terrestrial
301 LiDAR scanning (TLS) was undertaken. The topography of the site at the time of the excavation was
302 collected and the inner surfaces of the TP1506, 1507, 1510, 1511, 1512 were recorded. The LiDAR
303 scanner used for this survey was a Faro Focus 3D X-330. This is a short-range scanner (up to 300 m)
304 with an accuracy of ± 2 mm, a measurement rate of 997,000 measurements per second and an internal
305 high-resolution digital camera which enabled coloured point-clouds to be captured. The relative
306 distance, elevation angle and azimuthal angle between the LiDAR and the survey objects were
307 measured semi-automatically during each scan and, once processed, a 3D surface model was
308 generated. A series of locations around the site were chosen as either scan positions (5; see Figure 1a
309 and Figure 3a) or target positions (12). These were surveyed using a Leica GS14 Global Navigation
310 Satellite System (GNSS), a 120-channel receiver with an accuracy of up to 3 mm. This method relies
311 on the accurate positional control of the GNSS and the use of spherical prisms (Figure 3c),
312 checkerboard targets and planar surfaces as markers by which to 'tie' the scans together. At least four
313 of these markers need to be visible in every two adjacent scans, meaning that at least 8 markers were
314 visible in each separate scan, i.e. four markers visible to both scans 1 and 2 and four markers visible to
315 both scans 2 and 3 (scan 2 sees both sets of markers). The reader could refer to English Heritage
316 (2010) for hands-on guidance on how this is done in the field.

317 The LIDAR data produced by the oriented laser scan and GNSS survey were processed to develop a
318 Digital Surface Model (DSM) in Scene, Faro's acquisition and processing software. The raw data
319 produced by the Scene software consisted of a point-cloud comprising 900 million x, y, z points. These

data were oriented using the GNSS control positions and the markers. The output is an American Standard Code for Information Interchange (ASCII) file, made up of x, y, z, intensity and Red-Green-Blue (RGB) colour values. Therefore, each point of the cloud is attributed not only the relative x, y and z position in the three-dimensional space, but also the intensity of the reflected signal. Intensity is the amount of signal that has been reflected by the object surface hit by the laser of the LiDAR instrumentation (for further information see English Heritage, 2011).

The scans were then imported into Maptek I-Site Studio, point cloud processing and modelling software. From these data the DSM was generated across the whole site. Highly-detailed coloured point clouds of each trial pit were inlaid into the DSM (see Figure 9).

For each of the scanned TP, three products have been generated:

(i) the cleaned and processed point cloud;

(ii) the 3D model of the rendered surfaces;

(iii) the cloud intensity.

The latter output allows visualisation of the scanned surfaces based on the measurements of the magnitude of the reflected signal. According to the physical principles of LiDAR backscattering (Pfeifer et al., 2007; Krooks et al., 2013), intensity is also a function of the incidence angle with which the LiDAR laser hits the object surface. Some authors claim that this is a minor component of the intensity when imaging natural surfaces (Burton and Wood, 2010). Nevertheless, it is worth noting that differences in incidence angle and the resulting intensity are also due to different dip and surface roughness (i.e. asperities and protrusions) of the features observed over the stratigraphic sections within the TP. Therefore, using this LiDAR information, features across the stratigraphic column can be better enhanced and differentiated. In agreement with Challis et al. (2011), the intensity is used here as a surface descriptor of the earth material properties, to complement with the observations and feature detection undertaken by using the corresponding point cloud and 3D model. Section 4.4 demonstrates the benefits of processed TLS scans for better delineation of

geological features such as boundaries between contiguous strata, laminations, glacial and peri-glacial features, inhomogeneity in the grain size.

4 RESULTS

4.1 LiDAR-based palaeo-geographic understanding

At the landscape scale the DTM of the River Trent region confirms the flattish morphological setting of the environment where Farndon Fields is situated (Figure 4a). Compared with the topography of the surrounding countryside, this area at the current confluence of the Rivers Trent and Devon should have offered an ideal corridor to hunter community in LUP. According to the reconstruction based on the BRITICE database (Clark et al., 2004) and the very recent multi-stage recession model by Fairburn and Bateman (2016), Farndon Fields was likely formerly located towards the southern margin of the Glacial Lake Humber.

A close up of the site area enhances the extent of the terraces and the edges of the Holme Pierrepont Sand and Gravel Member which enclose Farndon Fields (Figure 4Figure 4b). At the northern end of the fields surveyed by FARI since 2012, the DTM shows a topographical high of about 13.4 m above OD. This is currently partially obscured by the junction of the A46 with the Farndon roundabout (feature B in Figure 4b). As the majority of the study area lies at lower elevation of about 12 m to 11.6 m OD, this topographic high is one of the most distinctive features that could have been observed before the A46 construction. Interestingly, the A46 embankment seems to have exploited this topographic high as a platform, alongside the other strip of higher elevation just south of the fields investigated in 2015.

Another interesting feature that might relate to the palaeo-environment of Farndon is a curvilinear area of lower ground to the east of the A46 and field 373B (feature C in Figure 4b). Pending the results of targeted site investigation, it cannot be excluded that this pattern represents the remnant of a former meander loop of the River Devon. Additionally, as recently noted by Garton et al. (2015), old aerial photographs (e.g. Royal Air Force oblique image taken in April 1947, reference RAF_CPE_UK_2009_4418) and historic maps provide evidence of a former braided Holocene

channel running towards the River Devon. These channels are not currently visible from above, even in recent false-coloured IR images (Figure 5; see section 3.3 for the image reference). The only other curvilinear feature that can be observed in this recent image is about 500 m SE of Farndon Fields. This evidence would suggest that features, once more distinctive, are progressively vanishing as the landscape is modified by contemporary human activities.

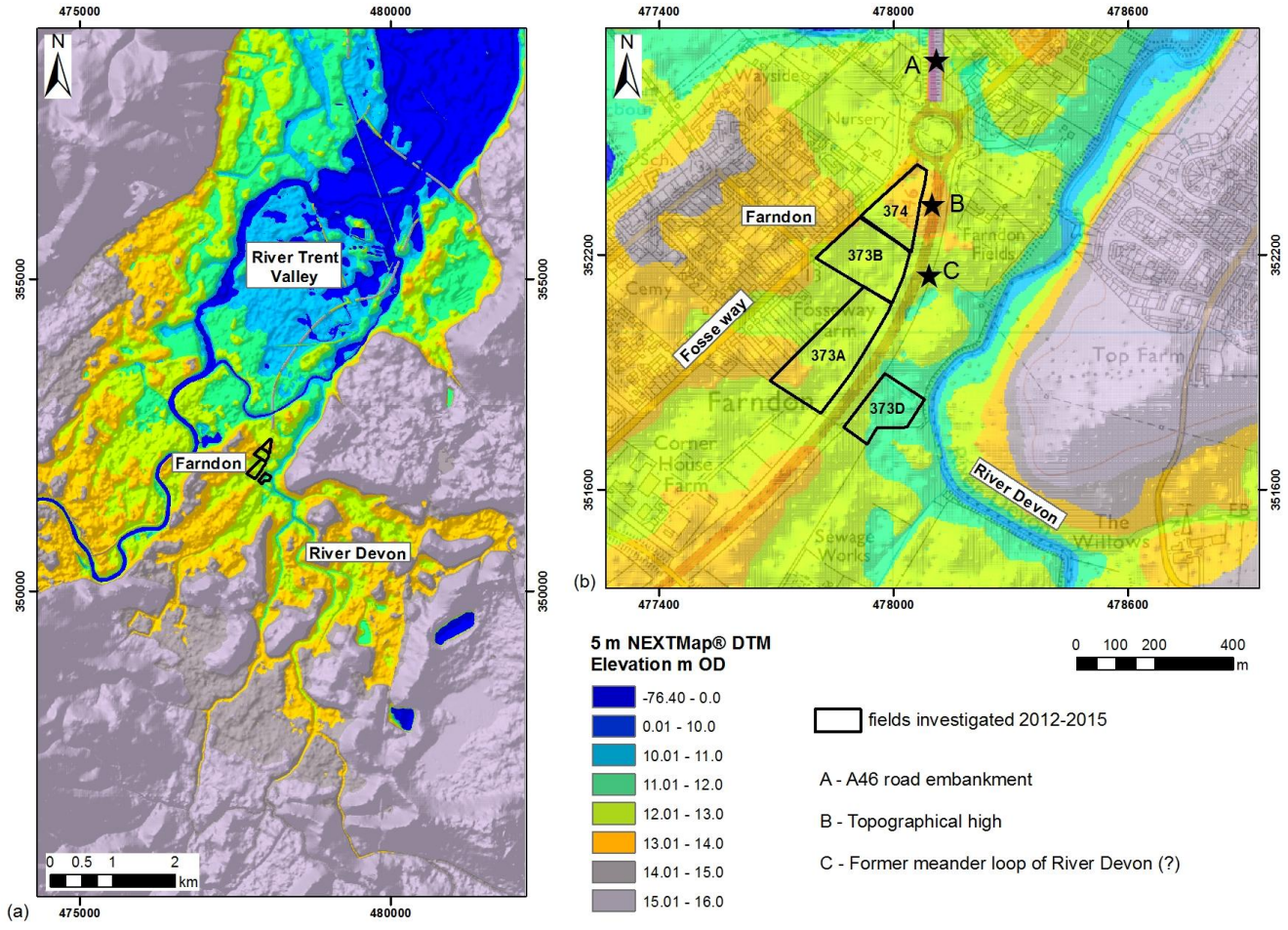

Figure 4 – Digital Terrain Model (DTM) of (a) the Trent region around Newark and (b) Farndon Fields based on 5-m NEXTMap® DTM. British National Grid; Projection: Transverse Mercator; Datum: OSGB 1936. Vertical Datum: OSGM91. Contains OS data © Crown Copyright and database rights 2016. NEXTMap® Britain © 2003, Intermap Technologies Inc., All rights reserved.

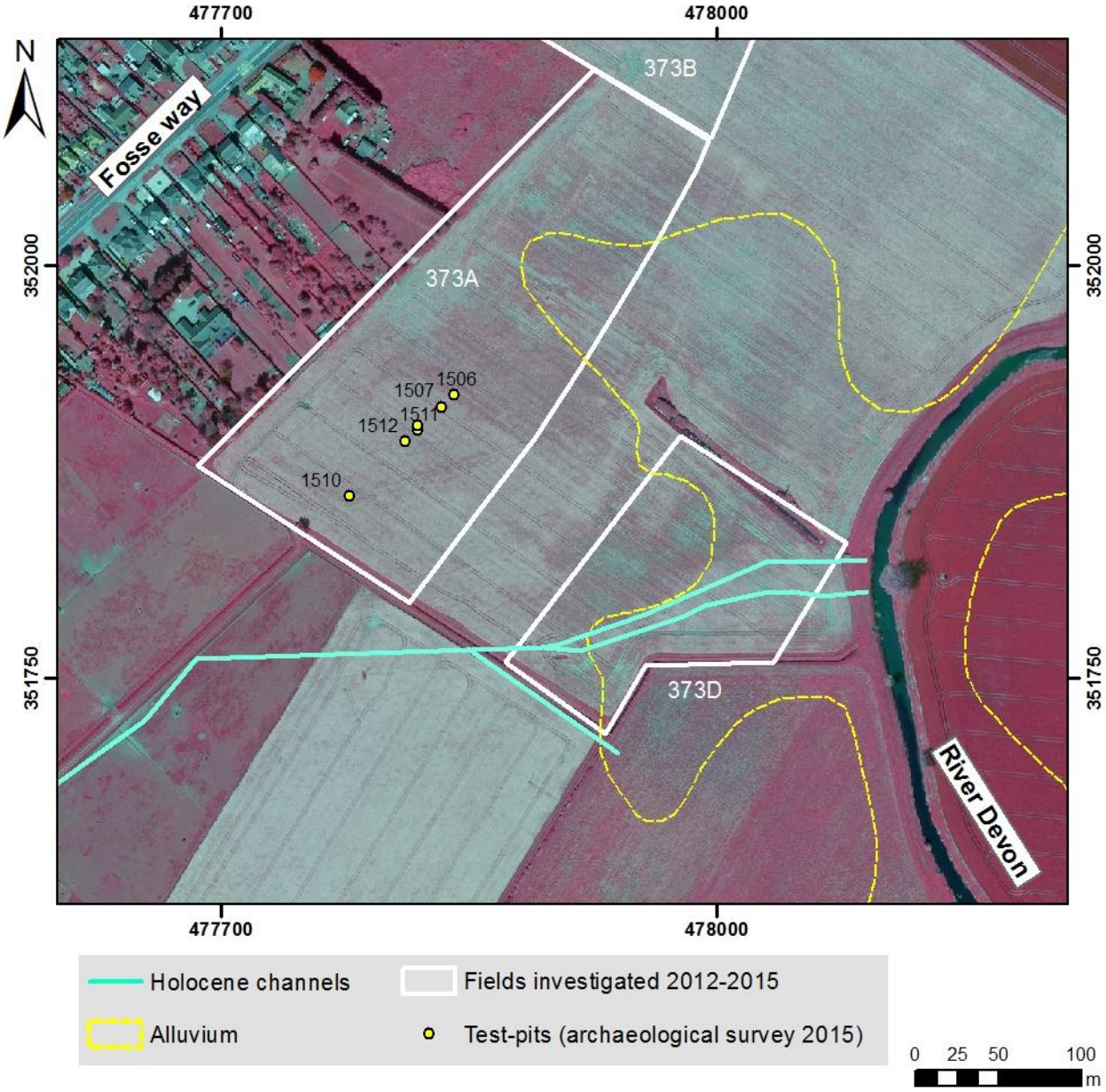

382

383 **Figure 5 –** False-coloured IR aerial photograph depicting the condition of Farndon Fields in May 2007 (photo
384 reference: PGA_SK7751_2007-05-01, licensed to BGS). The false-colour is obtained with the following
385 combination of the Red, Green and Blue (RGB) channels: near infrared light = red channel (R); red light =
386 green channel (G); green light = blue channel (B). The extent of the alluvium is derived from BGS' DiGMapGB
387 at 1:10,000 scale (BGS, 2016a; see also Figure 2a). The W-E track of the Holocene palaeochannel is drawn
388 based on old aerial photographs taken since 1933 (Garton et al., 2015, 109-110). Another palaeochannel
389 oriented NW-SE is drawn based on field data from Harding et al. (2014). British National Grid; Projection:
390 Transverse Mercator; Datum: OSGB 1936. Aerial photography © UKP/Getmapping Licence No. UKP2006/01.
391

4.2 Stratigraphy

Figure 6 shows the stratigraphy derived from in-situ observations and recording within the TP. At a first glance, the most noticeable feature is the topographic gradient of the full stratigraphy of sediments from SW to NE. This provides a stratigraphic confirmation of the surface topography measured from the airborne LiDAR data (see Figure 4b).

Below the modern ploughsoil largely consisting of humus (Figure 7a-b and Figure 8a-b), all the TP show a thick body of sands – hereinafter referred to as coversands – varying in colour, from brownish shallower strata to pale yellow deeper sediments. Predictably, the highest strata are more bioturbated and affected by reworking due to repeated farming activities, although bioturbation affects most of the coversand body and constrains its visibility. The best and deepest exposure of the coversands is found over the western face of TP1512 (Figure 7a).

The dark brown clayey silty sandy sediments underlying the coversands are interbedded with paler laminae, more silty at touch and which are very distinctive, as shown in TP1510 (Figure 7b) and TP1511 (Figure 8a) – they are here referred to as “laminated sediments”.

Between TP1513 and 1511 there is a step in the profile of the gravel terrace; the sediments are deepest around TP1511 and 1512. Pale polygonal cracking is visible in the terrace deposits at the base of TP1511; this might have been produced by freeze-thaw cycles of the ground. The cracks were subsequently infilled with fine sand. Vertical frost cracks run continuously from the sand and gravel deposits, through the laminated sediments and then into the overlying coversands (Figure 8a).

Pea-grit stringers are found within the laminae in most of the TP. During the survey, they were recorded at variable depths within the laminated deposits, sometimes forming distinct horizons which could be seen in section and sometimes visible only as sparse spreads whilst trowelling. In TP1511 the pea-grit is quite well sorted, thus suggesting a winnowed, higher energy flow event (see also LiDAR elaboration in Figure 17). In this regard, it is worth acknowledging that the environmental interpretation of the sediment units is ongoing and beyond the scope of this paper.

418

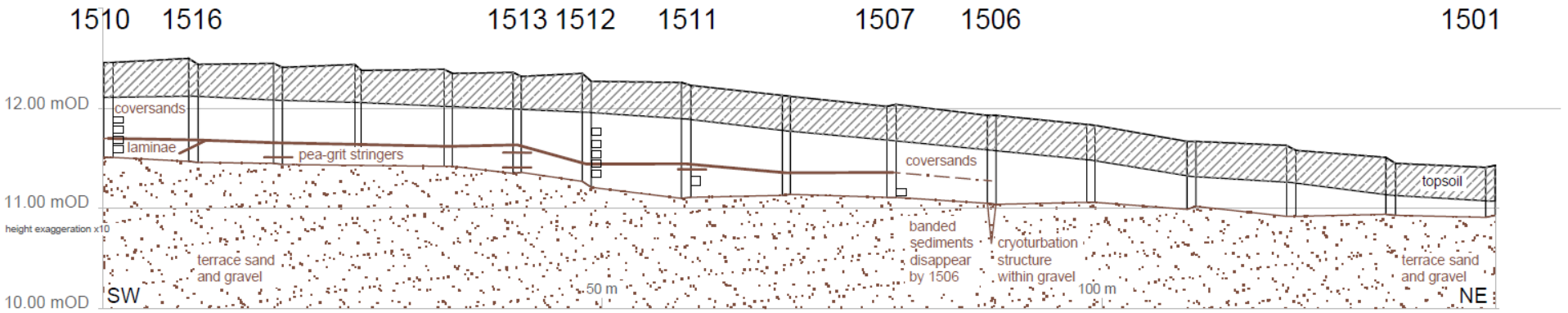

419

420 **Figure 6 –** Stratigraphic profile of the test-pitting transect A-A' excavated and investigated in September 2015 (see location in Figure 3a), with position of the TP
421 and location of the sediment samples. Height exaggeration x10; depths provided in metres above OD (elaboration by Daryl Garton).

4.3 PSA characterisation of the sediments

Table 3 summarises the grain size properties of the sediment samples from Farndon Fields (see also Table 2), alongside their moisture content determined in drying oven. The respective grain size distribution curves are displayed in Figure 7 and Figure 8.

The two sequences sampled in parallel, in TP1510 and TP1512, show quite consistent PSA values. In both cases, the sediments are mostly poorly graded sands, with coarse fraction retained on the 63 µm sieve not less than 58%. Higher percentages of finer fraction are found at deeper depths. The grain size distribution curves of samples #1 and 2 in TP1512 and samples #6 and 7 in TP1510 (see also Table 2) are characterised by a finer fraction tail (silt and clay; Figure 7c-d). A marked separation is then observed from sample #2 to sample #3 and from sample #7 to #8, when the clay fraction decreases markedly.

Calculations of the inclusive graphic skewness (Sk) for the coarser fraction according to the methods and nomenclature by Folk (1974) highlight that samples #1, 2, 6 and 7 are all strongly negative skewed, with consistent Sk values close to -1.0. Similar figures are also retrieved for samples #10 and 11 which are stratigraphically located within the laminated sediments (Figure 6 and Figure 8a-b) and both show fine fraction tails (Figure 8c).

As for the moisture content (Table 3), the highest value measured is about 13% and was found in sample #6, i.e. located at the bottom of TP1510 and corresponding with the highest percentage of clay fraction (22.5%), whilst the lowest moisture content (3.5%) corresponded with the lowest percentage of the clay fraction (5.0%) in sample #3, towards the middle of the coversands.

444 **Table 3 –** Summary of grain size properties of the samples from Farndon Fields (see also Table 2). Notation:
445 Maximum size of the smallest 10% (d_{10}), 30% (d_{30}) and 60% (d_{60}) of the sample; Coefficient of uniformity (C_u),
446 Coefficient of curvature (C_c).

447

Sample	Grain size properties									
	Gravel [%]	Sand [%]	Silt [%]	Clay [%]	D_{10}	D_{30}	D_{60}	C_u	C_c	Moisture content [%]
1	0.1	69.4	13.8	16.8	-	0.063	0.200	-	-	8.7
2	0.2	78.3	11.5	10.0	0.002	0.100	0.250	125.00	20.00	5.7
3	0.0	76.1	18.8	5.0	0.015	0.100	0.225	15.00	2.96	3.5
4	0.1	69.2	23.5	7.2	0.006	0.063	0.180	30.00	3.68	4.1
5	1.1	70.5	19.9	8.5	0.004	0.070	0.200	57.14	7.00	4.5
6	0.4	58.3	18.8	22.5	-	0.015	0.120	-	-	13.3
7	0.2	67.4	16.0	16.4	-	0.045	0.160	-	-	9.4
8	1.0	74.4	17.1	7.5	0.006	0.080	0.195	35.45	5.97	6.3
9	0.7	72.0	18.4	8.9	0.003	0.070	0.190	63.33	8.60	7.3
10	0.1	69.9	12.5	17.5	-	0.063	0.180	-	-	8.9
11	0.8	55.4	26.3	17.5	-	0.015	0.125	-	-	8.1

448

449

450

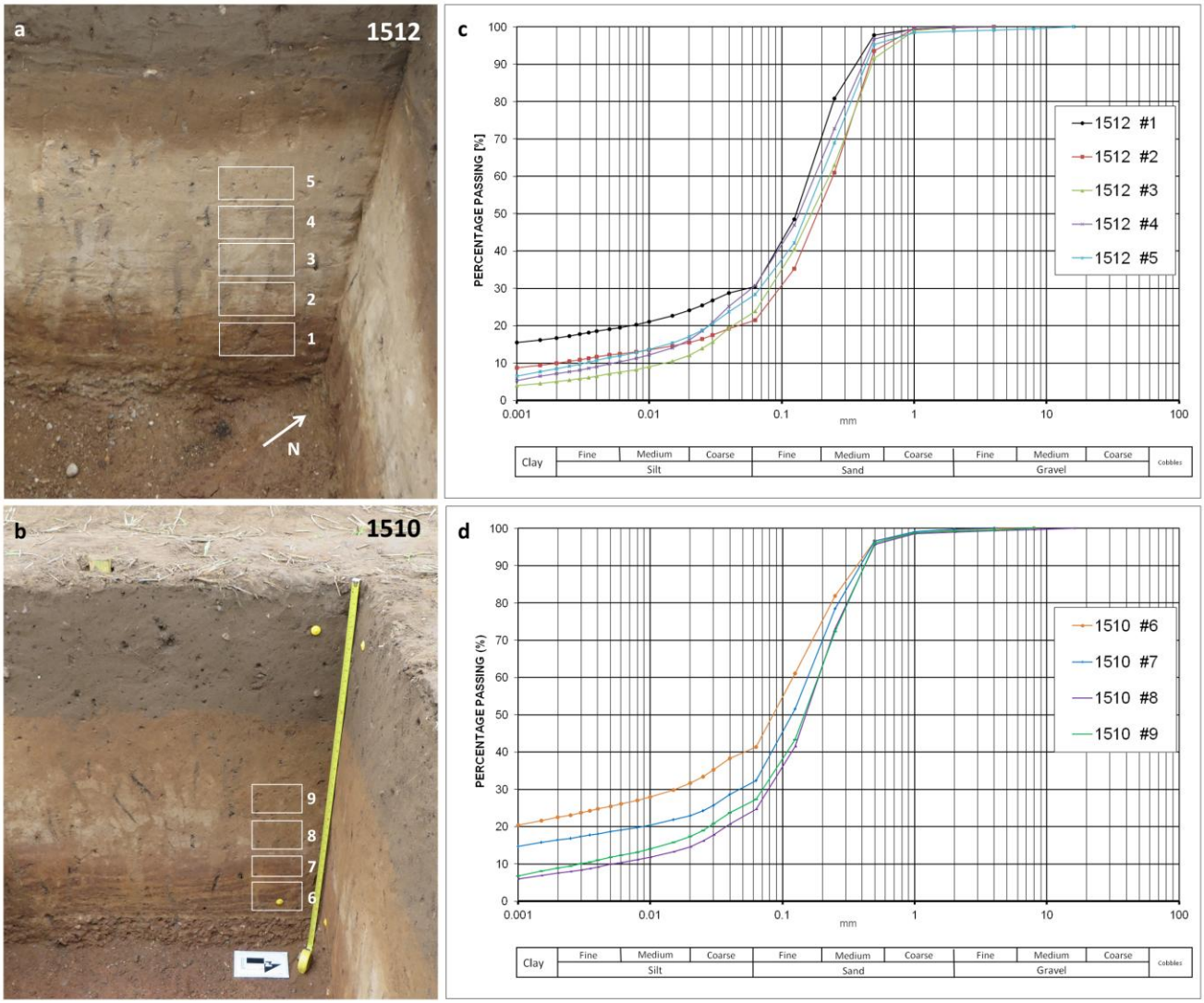

451

452 **Figure 7 –** View of the western cross-sections of TP (a) 1512 and (b) 1510, with location and numbering of the
453 samples taken in September 2015; (c-d) respective grain size distribution curves (Photo credits: David Budge
454 and Deodato Tapete).

455

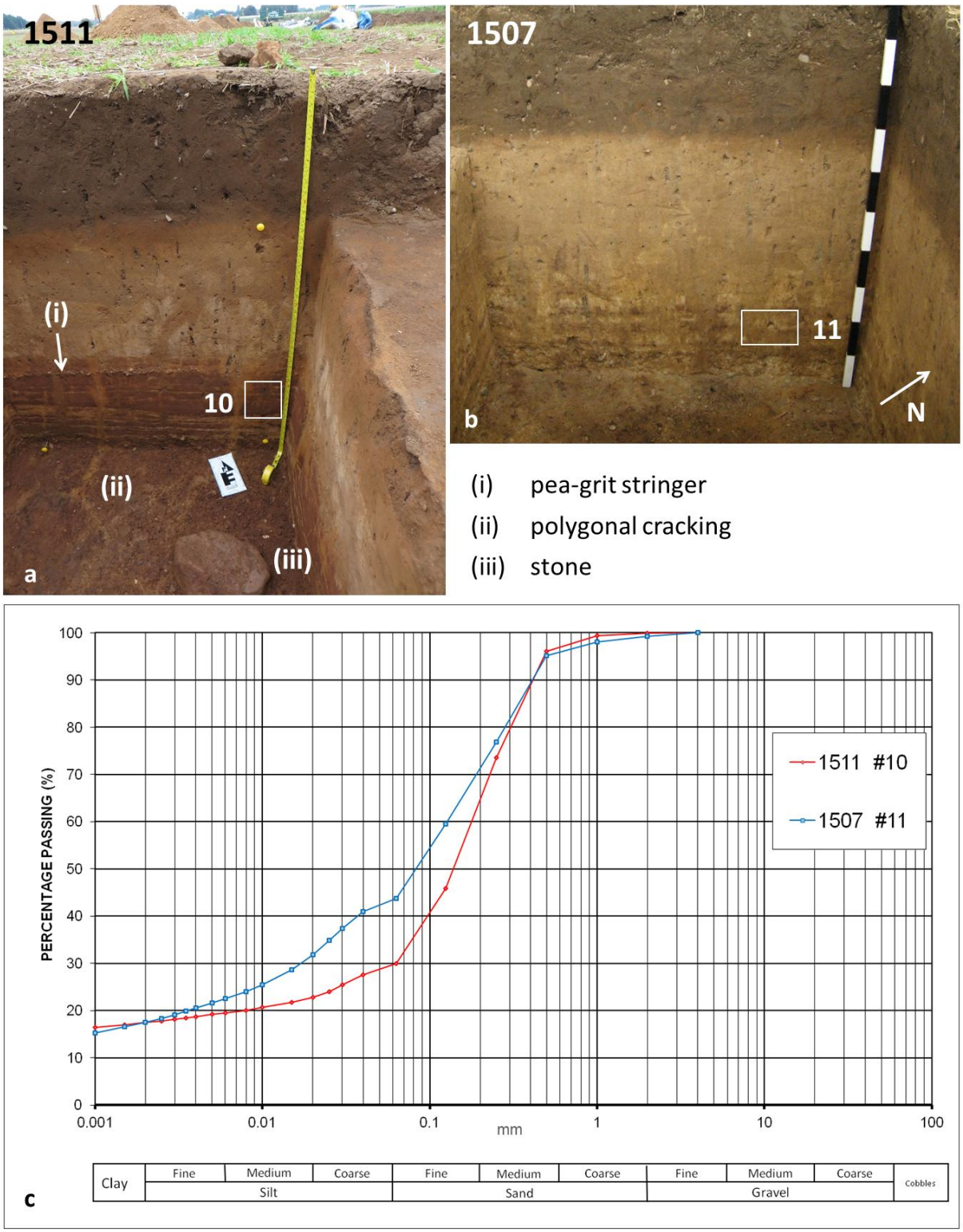

Figure 8 – View of (a) the western cross-section of TP1511 and (b) northern face of TP1507, with location and numbering of the samples taken in September 2015, as well as indication of: (i) pea-grit stringer; (ii) polygonal cracking; (iii) the stone found at the bottom of the pit. (c) Respective grain size distribution curves (Photo credits: Deodato Tapete and Daryl Garton).

4.4 Geological profiling and feature detection from Terrestrial LiDAR Scanning

Figure 9 shows the Digital Surface Model (DSM) of Farndon Fields which provides a very high resolution 3D record of the local topography at the time of the archaeological survey. As specified in section 3.4, the DSM was generated by bringing the completed scan data into the 3D point cloud processing software package Maptek I-Site Studio. Vegetation, isolated and un-related points that were random and did not belong to the environment (e.g. due to operators working in the field, animals, objects) were removed. To this purpose, a routine series of filtering tools was applied. The individual scans (see 3D models in Supplementary materials) were then merged into a single feature scan (Figure 9).

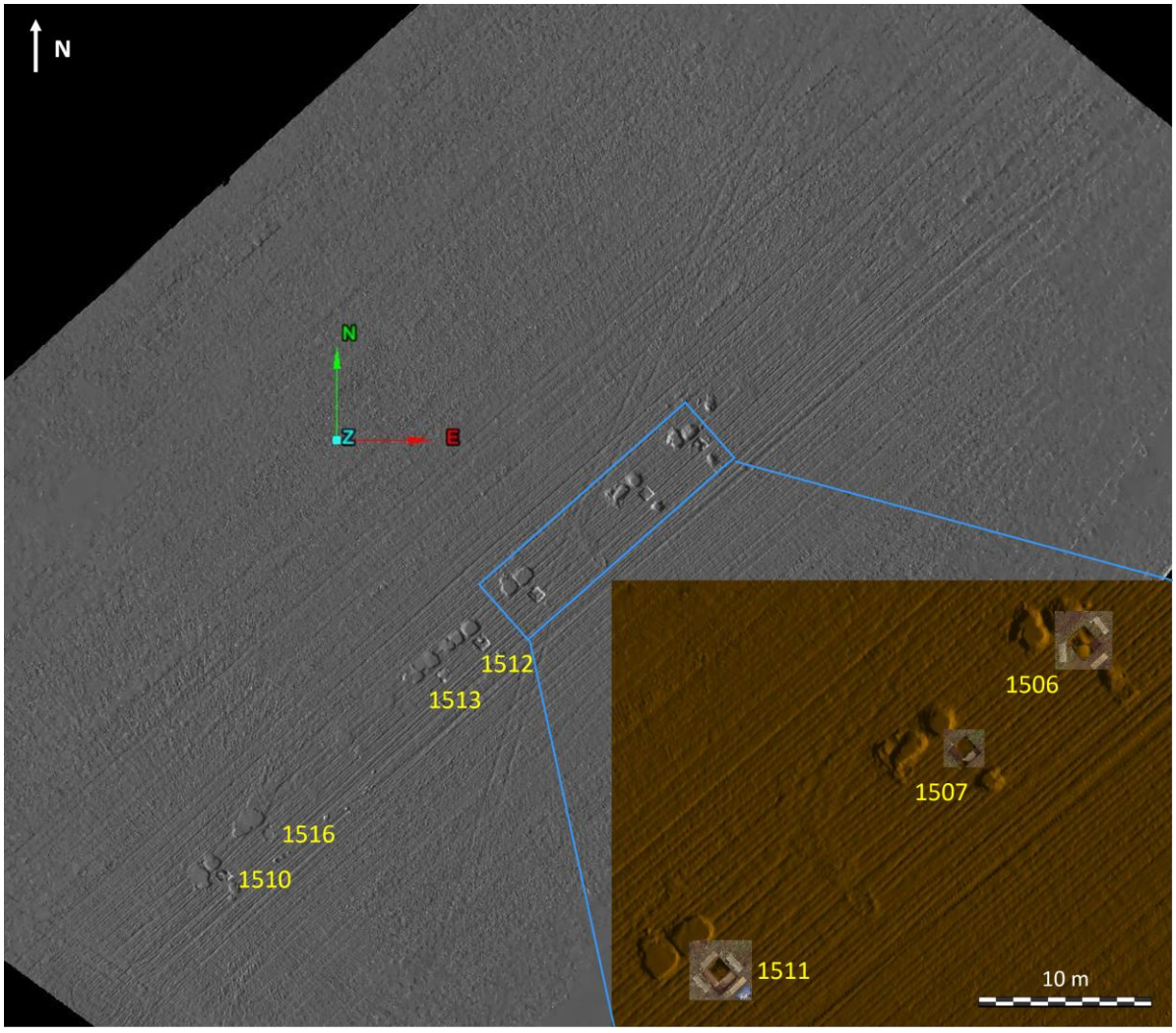

Figure 9 – Farndon Fields Digital Surface Model (DSM) with coloured point clouds of the TP superimposed. BGS © NERC. All Rights Reserved 2016.

From this detailed DSM it is apparent that neither topographic anomalies nor shallow marks suggesting the presence of buried features of archaeological or geological relevance can be observed in the landscape where the TP were dug. Indeed, the maximum elevation variation measured with regard to the scanned TP1506 in the north-east and TP1510 in the south-west along transect A-A' is about 0.6 m. As expected, the highest values coincide with the temporary mounds of excavated soil close to the TP.

The scan points making up the individual TP were highlighted and laid above the DSM. This combined digital product will serve in future to retrieve the exact position of the TP and indicate the presence of ground disturbed by the archaeological excavations. For the purposes of this research, the coloured point clouds acquired and processed for the five TP are used to undertake a holistic analysis of the TP as if they were part of a virtual excavation trench.

Figure 10 shows the Red-Green-Blue (RGB) colour and grey-scale intensity images of TP1510. The TP is viewed from the south to achieve a full visibility of the northern and north-western cleaned faces and the floor of the pit. The colour contrast in the RGB image and the marked difference of intensity return in the intensity image were used to determine and draw the geological boundaries between the coversands and the overlying ploughsoil and the underlying laminated sediments in all the TP. To connect each TP with the next one, a series of points were marked on the inner faces of the pits at the depths where the same geological boundary between the sediment units was found. Then a surface was interpolated between these points and a series of 0.2 m contours were created (Figure 11).

The result is a geological profile (Figure 11) which matches the cross-section drawn using traditional techniques (see Figure 6). The advantage is that this geological profile is digital, three-dimensional and can be rotated and interrogated. As we move along A-A' transect from the TP1510 to TP1506, the same sediment units are found at deeper depths, thereby resulting in a topographic gradient with total dip angle up to 2° (Figure 11).

3D rotation of this virtual geological profile allows an enhanced understanding of the horizontal and vertical distribution of the archaeological and geological deposits within the x-y-z space. Furthermore,

by means of interpolation, it is also possible to predict the location and depth where the various strata are expected to be found in the gaps between the scanned TP and corroborate the archaeological stratigraphic model of the study transect in Farndon Fields (see also section 4.2).

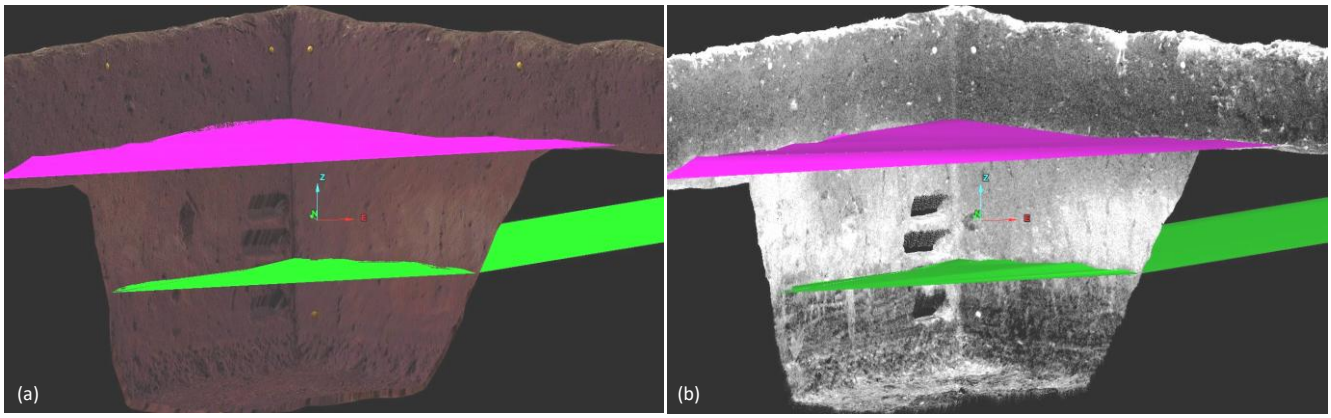

Figure 10 – (a) RGB and (b) grey-scale intensity images of the TP1510 showing the geological boundaries of the coversands (purple) and laminated sediments (green) layers. BGS © NERC. All Rights Reserved 2016.

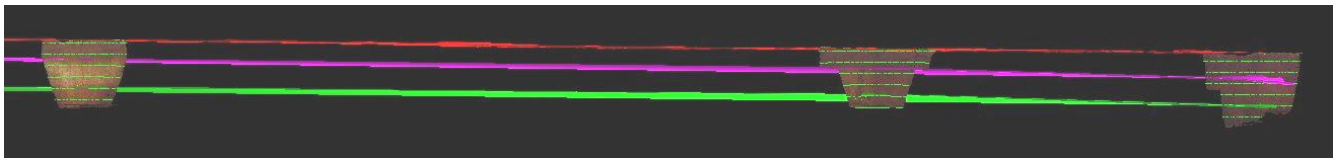

Figure 11 – DSM of the ground surface (red) and interpolated surfaces of the coversands (purple) and laminated sediments (green) layers, for three of the five scanned TP. BGS © NERC. All Rights Reserved 2016.

The point cloud data of each TP were processed into the software package Cloud Compare and classified by intensity and roughness values. Roughness is here referred to as the distribution of the heights of asperities and protrusions of the inner surfaces of the TP. Asperities and protrusions are defined with regard to a smoother reference surface that has been chosen as the datum.

Figure 12 displays the output of the intensity classification for TP1510, according to a Blue-White-Red colour scheme using intensity thresholds of 1400, 1550 and 1600. Such classification proved to be effective across the TP to pick out the boundaries between the ploughsoil (blue) and the coversands (red), and between the coversands and the laminated sediments (blue), and therefore facilitate an automated calculation of the strata thickness and recognition of depositional and post-depositional

features. Using this classification technique and colour scheme, we found the evidence of a transition layer between the ploughsoil and the coversands (Figure 13) that was not visibly apparent or well delineated by either the naked eye or on the RGB coloured point cloud. This transition layer follows the upper boundary of the coversands without interruption, but its thickness varies across the TP. In particular, it ranges from 6 cm as observed in TP1511 (Figure 13) to 16 cm as measured in TP1512.

With regard to feature detection, the red intensity patterns in Figure 12 clearly mark the presence of infiltrations of the coversand as a pedological overprinting onto the underlying laminated sediments (see black arrows in Figure 12). This is another common feature of the scanned TP that was also recognisable by the naked eye but was seen with improved visibility due to the colour contrast characterising the exposed pit faces. Similar benefit from the use of intensity classification can be appreciated in the capability to delineate the inhomogenities and texture within the sediment units. For instance, it is possible to differentiate the laminations within the laminated sediments themselves (Figure 13), since the bands have average intensity of 1592 against 1478 measured in the surrounding matrix.

The intensity values are also extremely useful for looking at specific geological features, such as convolutions associated with the cryoturbation structure recognised by the archaeologists at the bottom of TP1506 (feature labelled (c) in Figure 14). Figure 15 demonstrates how the intensity image complements the RGB coloured point cloud in making more evident the morphology and texture of the cryoturbation, using in this case a bespoke Blue-Green-Yellow-Red colour scheme. This technique gives a precise record of the very complex sedimentary architecture developed under periglacial conditions. The morphology, as seen in Figure 15d, would suggest a classification of this structure to Type 5 according to Vandenberghe (2013).

Nonetheless, some features that are clearly visible with the naked eye are not picked up very well by the intensity classification, such as the ice crack feature or the pea-grit stringer in TP1511. In these situations the low intensity difference between neighbouring features acted to the detriment of feature discrimination. However, these features can be seen within the RGB coloured point cloud and, even

548 better, in the triangulated surface model (Figure 16). The explanation of such better performance can
549 be found in the enhancement of the local surface roughness and morphology as a consequence of the
550 process of surface triangulation. Surface roughness is a parameter stored in the point cloud that can be
551 extracted and classified to better delineate geological features. Using the tool available in Cloud
552 Compare to estimate the roughness, for each point the kernel, or centre point, is calculated. The
553 'roughness' value retrieved is equal to the distance between this point and the best fitting plane
554 computed on its nearest neighbours.
555
556

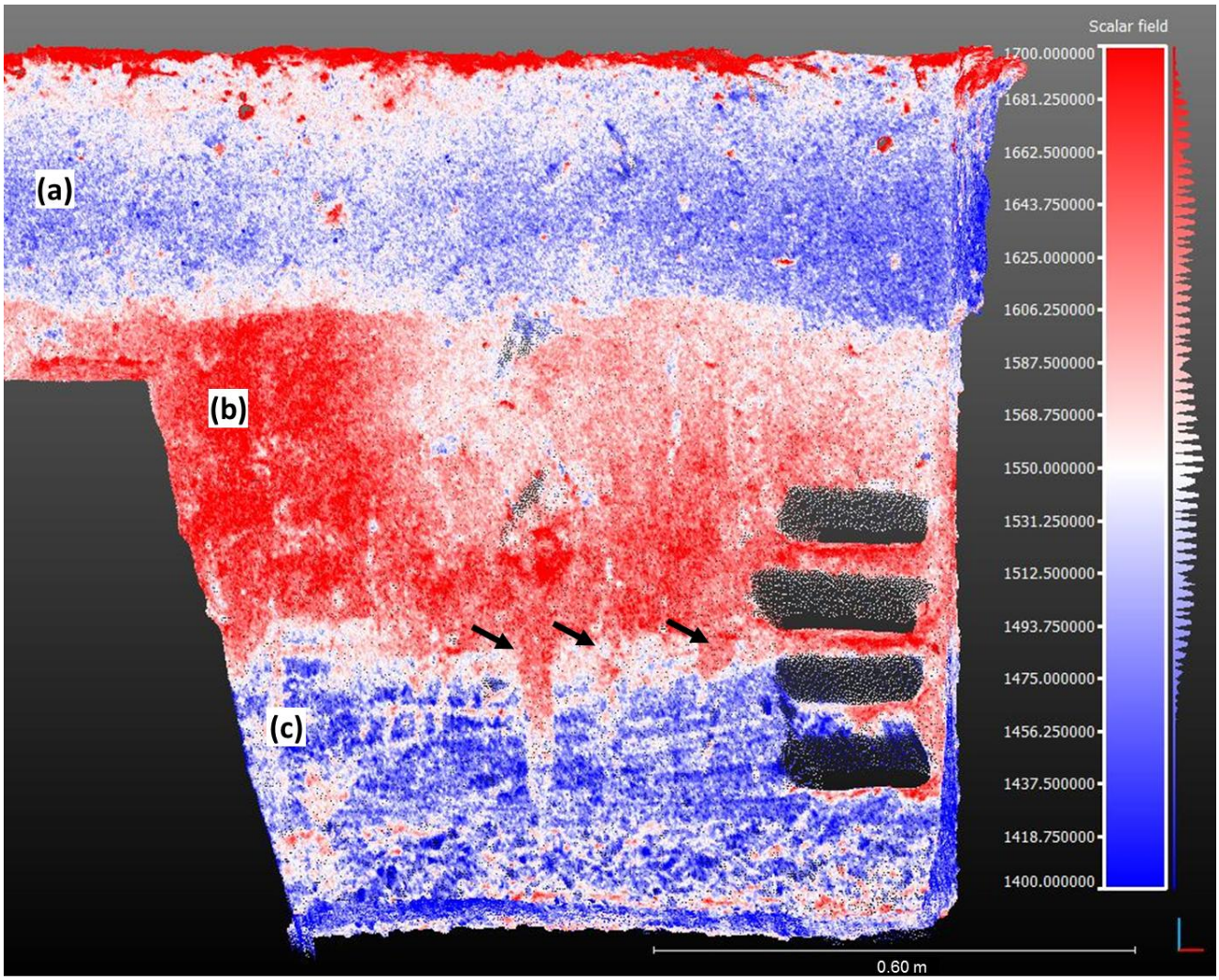

557

558 **Figure 12 –** Intensity classification of TP1510 based on Blue-White-Red colour scheme which allows the
559 discrimination, from top, of: (a) ploughsoil; (b) coversand body; (c) laminated sediments. Voids on the right are
560 the cavities left from the sediment sampling. Black arrows mark features due to infiltrations from coversands
561 into the laminated sediments.

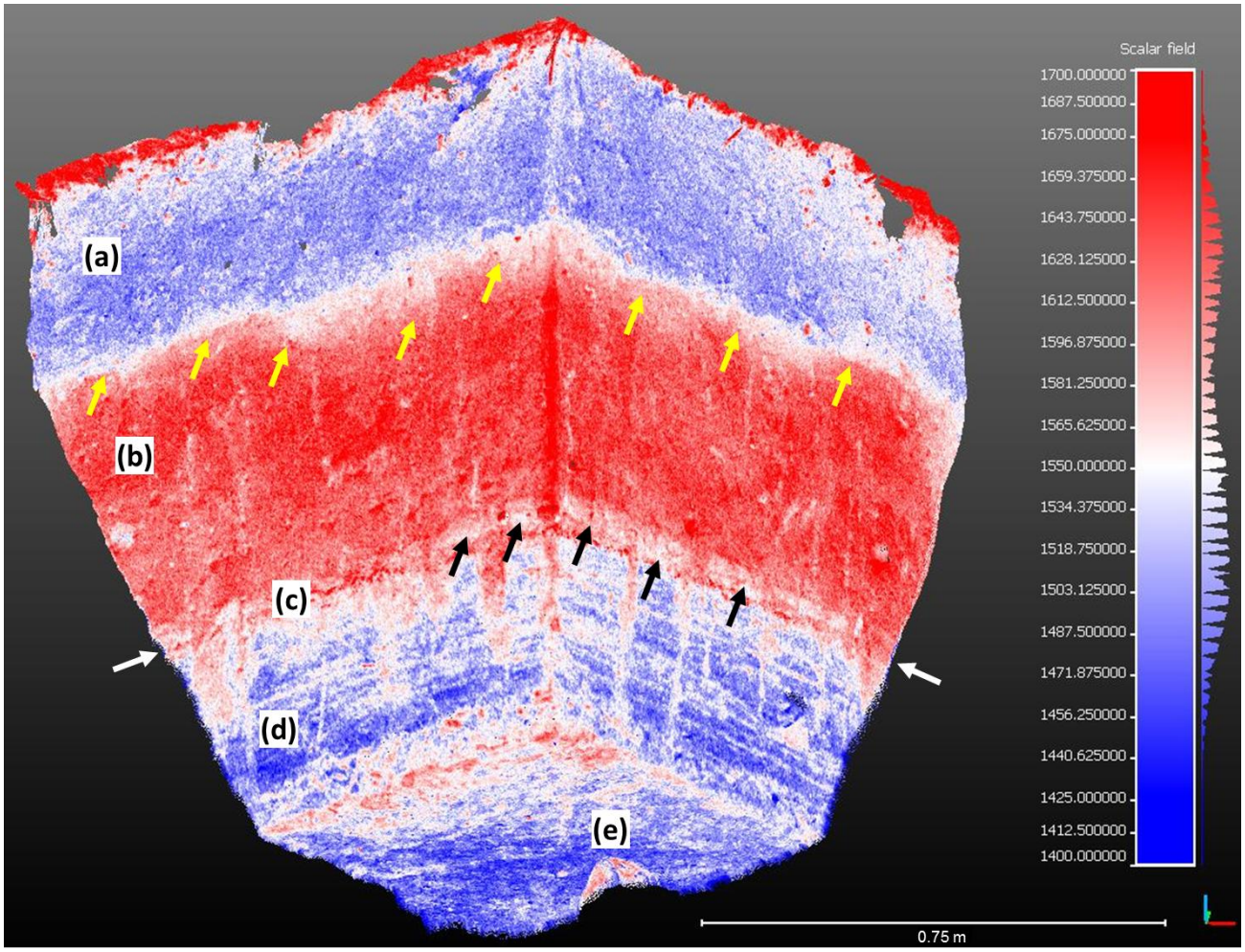

Figure 13 – Intensity classification of TP1511 based on Blue-White-Red colour scheme, with indication, from top, of: (a) ploughsoil; (b) coversand body; (c) pea-grit stringer; (d) laminated sediments; (e) stone at the bottom of the pit (compare with Figure 8a). Yellow arrows mark the transition layer between the ploughsoil and the coversands; white arrows point to each end of the pea-grit stringer; black arrows indicate a layer above the pea-grit stringer that shows distinctive intensity compared to the overlying coversand body.

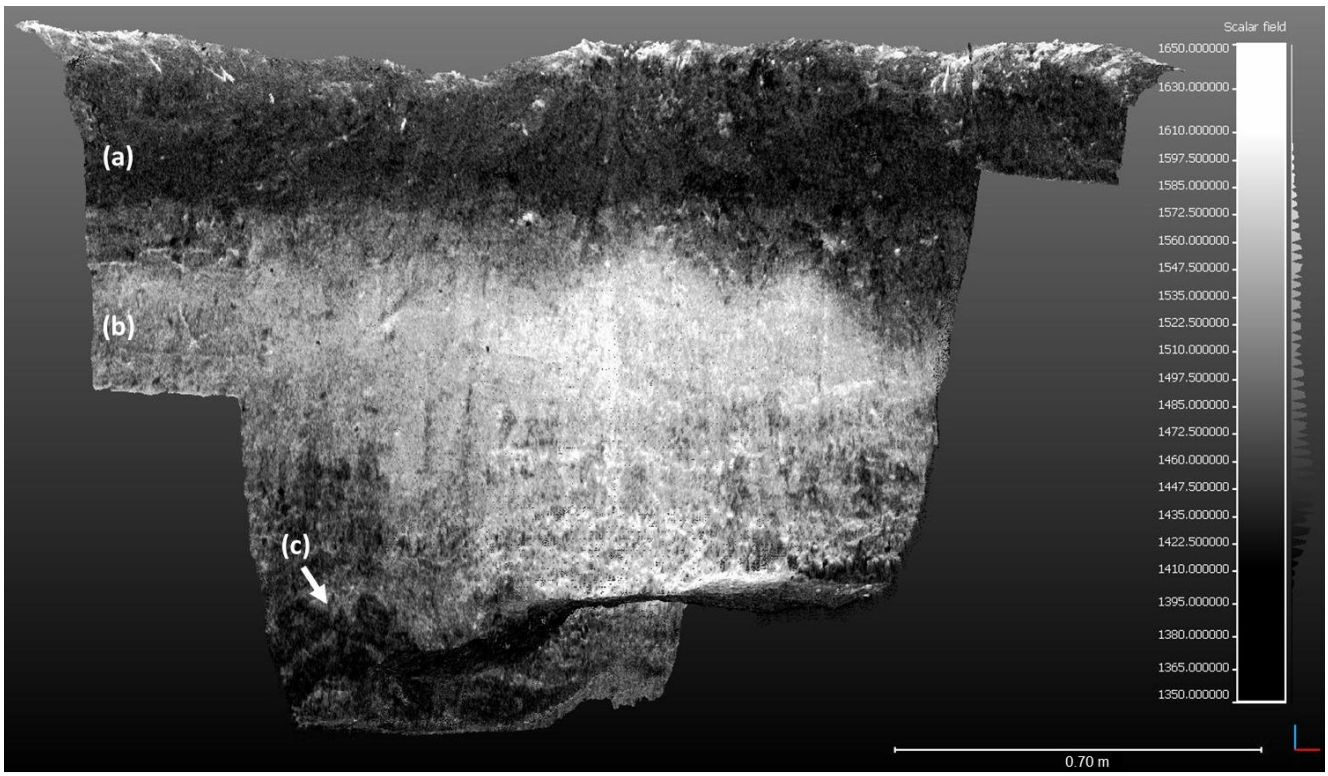

Figure 14 – Cloud intensity of the western and northern faces of TP1506, with indication, from top, of: (a) ploughsoil; (b) coversand body; (c) cryoturbation structure. The intensity returns reveal internal bedding of the coversands that is not visible with the naked eye.

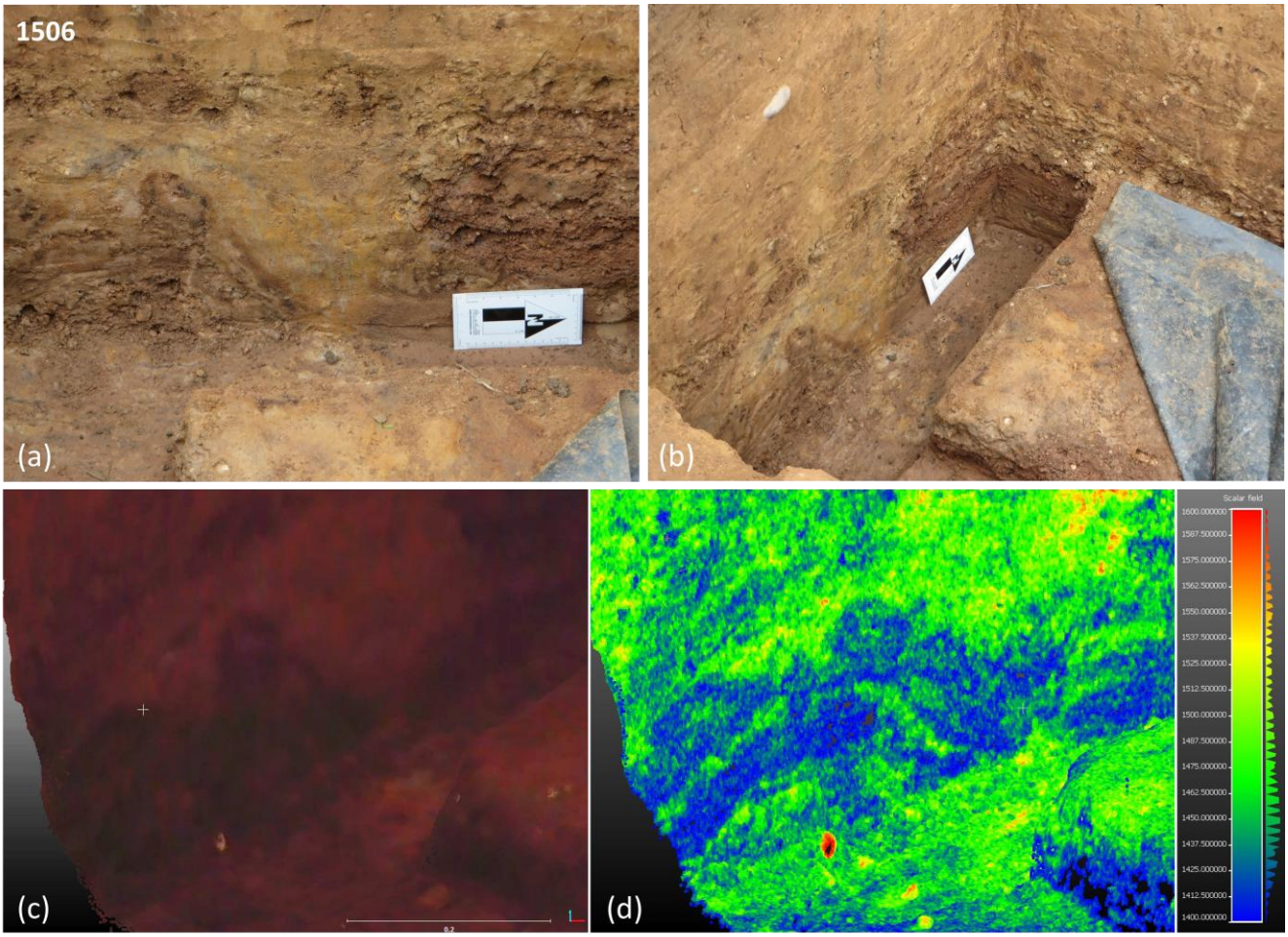

576

577 **Figure 15 –** Convolution feature associated with the cryoturbation structure found at the bottom of the
578 stratigraphy exposed in the western face of TP1506 viewed from (a) east and (b) south. (c) RGB and (d)
579 intensity images from the LiDAR scan processing. Scale bar at bottom right of picture (c) measures 0.20 m.
580 (Photo credits (a) and (b): Deodato Tapete).

581

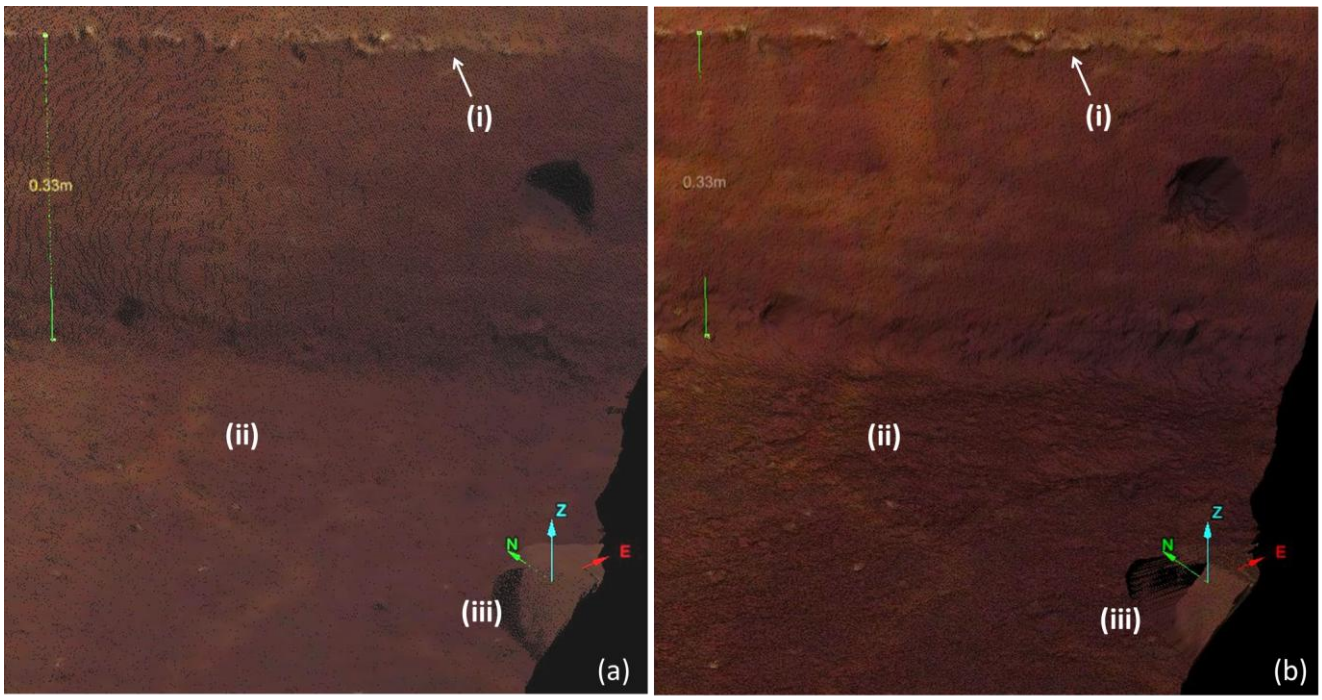

Figure 16 – (a) RGB coloured point cloud and (b) triangulated surface images of the bottom portion of TP1511, with indication of: (i) pea-grit stringer; (ii) ice crack feature; (iii) drop stone (compare with Figure 8a). Note that the circular feature on the right is due to the sediment sampling. BGS © NERC. All Rights Reserved 2016.

Figure 17 shows the results for TP1511. The pea-grit stringer close to the upper boundary of the laminated sediments is clearly picked out, thereby providing an effective way to automatically map its distribution and isolate it from the rest of the stratigraphy. The difference of particle size is apparent and this confirms that the pea-grit is quite well-sorted (see also section 4.2), a property that might contribute to unveil the type and energy of the environment when it formed. Other features such as the large drop stone on the pit floor and the sampling locations can also be identified. Nonetheless, limitations to an effective and selective discrimination by surface roughness are in this case due to: (i) the presence of bioturbation/cryoturbation within the coversands that randomly may be classified with similar value as the pea-grit; and (ii) the small gradient along the z-direction (i.e. along the direction orthogonal to the pit face) which may result in some features or parts of them being less clear in the surface roughness map. Of course the corners between the pit faces and the bottom appear rougher due to their geometry, but for the purposes of geological feature investigation they can be neglected and only used as a spatial reference within the x-y-z space.

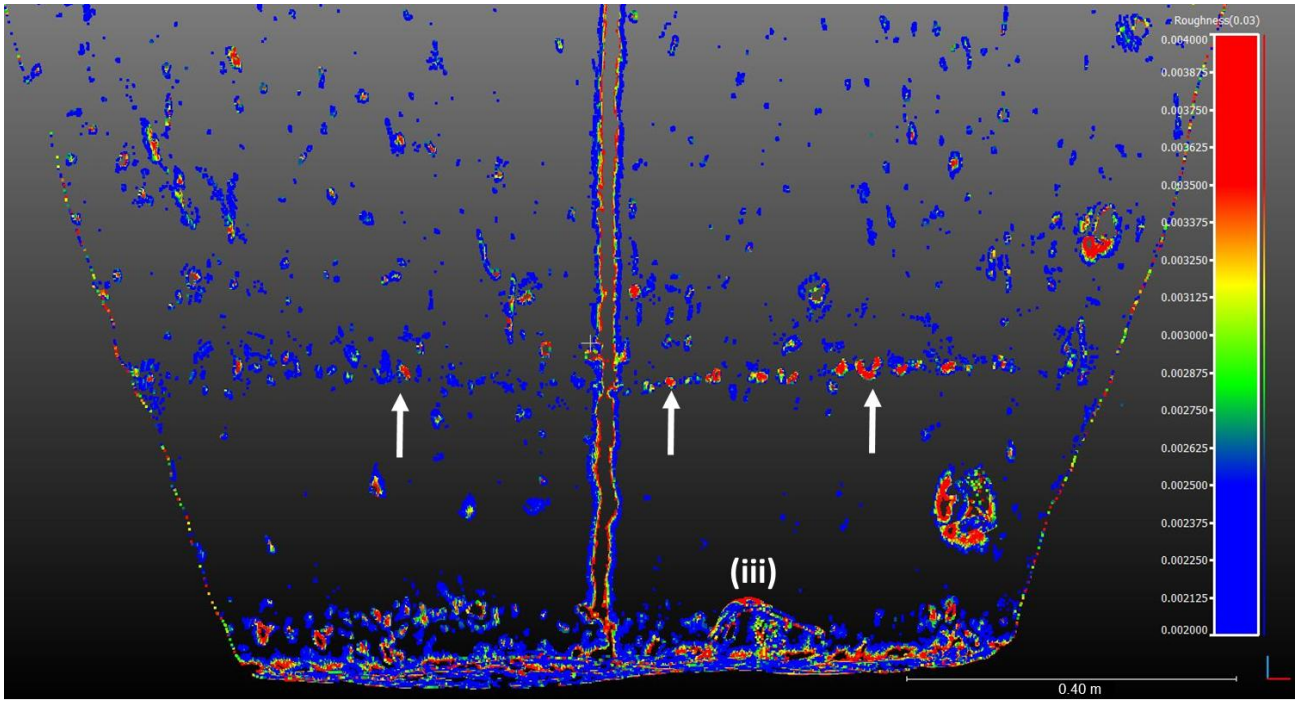

Figure 17 – Roughness estimate for TP1511 clearly showing the pea-grit stringer (white arrows). The drop stone on the pit floor is visible (iii; compare with Figure 16). BGS © NERC. All Rights Reserved 2016.

5 DISCUSSION

In the low lying area of the Trent Valley the extent of geology exposed, either as natural outcrops or human-induced exposure (e.g. quarry or excavation trenches), is scant. Such poor exposure of the geology contributes to the research challenges to reconstruct the palaeo-environment in Farndon Fields. Therefore, whilst being the only option available to archaeologists to build on the data obtained from augering, test-pitting was also an opportunity to upgrade the geological mapping through *in-situ* observation of the structure of the sediment profiles of this area of the River Trent region. This had been recognised by Garton et al. (2015) as a knowledge gap that this research aimed to fill by combining traditional methods (PSA and geological stratigraphic observations) and state-of-the-art LiDAR technologies for regional-scale assessment and local-scale data capture.

Airborne LiDAR DTM and aerial photographs were used for modelling of the morphological and topographic setting of an area around Farndon Fields that was chosen for repeated phases of occupation by hunter-gatherers during the Late-Glacial. In this location the longitudinal crest of the

Holme Pierrepont Sand and Gravel terrace-deposits is interrupted by low-lying land that would support the hypothesis of a floodplain and channel-edge environment where groups of hunters could find a corridor. This information is even more important if we consider that, in addition to the alteration due to farming activities, the site has been recently disturbed by the construction works for the A46 and new development is planned further south. Features of past landscape are already vanishing as multispectral investigation of the area based on false-coloured infrared images from above has demonstrated (Figure 5).

The geological and stratigraphic profile retrieved from the test-pitting clarifies the topographic conformation of the terraces, with a clear SW-NE gradient and a slight step between TP1513 and 1511. Strata of coversands overlie the laminated sediments found at the bottom of the test-pits and their thickness tends to decrease moving towards the NE along transect A-A'. Bioturbation affects the visibility and interpretation of the coversands. This is partially reflected in the PSA results with finer particles within the deeper strata (see section 4.3). Nonetheless, it is worth noting that consistent values and geotechnical parameters are retrieved for the coarser fraction of these sediments at matching depths along the stratigraphic column of the TP.

Whilst it is still matter of conjecture how best to interpret the laminated sediments lying below the coversands (this is outside the scope of this paper), terrestrial LiDAR scans provide new information that could not have been retrieved based on field observations with the naked eye. Intensity classification of the point clouds not only enhances the boundaries between the sediment units, thereby allowing a more precise stratigraphic separation, but also shows discontinuities and variations in the texture and surface roughness within each TP and across the whole test-pitting transect. In particular horizontal laminations and internal bedding of the coversands are observed (Figure 14) and this is completely new evidence that LiDAR technology has brought to light. This could not have been inferred from solely the PSA results. Despite the sampling selectivity, PSA does not appear to be enough sensitive to highlight the variability within same sediment units that, instead, is observed in the LiDAR scans.

Post-processing of the point clouds also proves the added value offered by the LIDAR scans to generate a digital geological profile matching with the traditionally recorded stratigraphic profile, with the functionality of extracting, delineating and measuring features of geological interest, such as the cryoturbation in TP1506 (Figure 15) and the pea-grit layer (Figure 17). It is apparent how this type of digital data can be helpful for desk-based studies and after the closure of temporary excavations, as they remove any ambiguity about the location of the stratigraphic features and samples, and provide a reliable record of the morphology of complex sedimentary structures.

6 CONCLUSIONS

The investigation at Farndon Fields demonstrates the benefits of phased investigation (archaeological and geological) as an approach to more cost-effective investigation of archaeological context through strategic sampling of landscape domains.

The analysis of the airborne LiDAR data demonstrates how detailed processing can be used to enhance the understanding of the landscape, e.g. the former distribution of water bodies through the analysis of the form of the low lying ground. The geological data, including the mapped extent of alluvium and the detail recorded on the 1:10,000 field slips form the foundation of this understanding.

At Farndon Fields, the increased resolution of the observations that result from test-pitting, and the new technologies deployed to record and analyse them, have provided an added level of confidence to our ability to discriminate between the laminated sediments, coversands and ploughsoil.

The intensity cloud processing demonstrates that this technique works very well to highlight internal structure in the sediments that would not have been otherwise detected by the naked eye. The roughness index also shows considerable potential for recording the grading of the sediments. The ground based LiDAR results provide a reliable record of the depositional structures (lamination and banding) and grain size that characterise the geological units in the test pits. Although as yet incomplete, the enhanced detail facilitates better interpretation and discrimination of the nature and phasing of the post depositional environmental factors that have affected the strata, such as

669 cryoturbation (e.g. ground cracking and water escape features) and bioturbation processes as well as
670 anthropogenic weathering and erosion, including the depth of ploughing and the compaction and
671 consequential increase in soil density that results from ploughing.

672 It is clear that this type of technology has the potential to support palaeo-environmental research at
673 Farndon and elsewhere as it provides a robust, digital record that can be manipulated and used to
674 capture the detail of both the sediment architecture and the position and timing of any sampling and
675 testing.

676 Further advance of the research might be to test LiDAR to discriminate between different grading
677 and particle size, but there is the question whether the particle size of these deposits is too fine to be
678 determined by this type of LiDAR, consequently we still rely on traditional methods such as PSA and
679 therefore will continue to need to collect samples. Hand-held LiDAR might provide a technological
680 solution, for example the fact that the pea-grit was clearly detected and extracted as a stratigraphic
681 feature from the LIDAR point cloud is encouraging.

682 Certainly, the current regional interpretation would benefit from more sampling and more spatial
683 understanding of the heterogeneity of the grading of the sediments, and this would benefit from the
684 techniques that have been demonstrated during the September 2015 phase of test-pitting. Used at the
685 regional scale, with processing being undertaken as an integral part of the investigation as it proceeds,
686 these techniques offer significant potential for planning strategic cost-effective sampling.

687 This research has confirmed the challenges associated with establishing *in-situ* subsurface buried
688 terraces, where the modelling of the former landscape will help to predict the location(s) where *in-situ*
689 contexts for the archaeological finds might be preserved at Farndon Fields.

690 Investigations of this type offer significant potential for improving the resolution of the geological
691 detail, particularly where archaeology converges with geologically significant sites, e.g. in the case of
692 Farndon Fields, towards the southern edge of the potential former Lake Humber.

693

ACKNOWLEDGEMENTS

The research presented in this paper was carried out in the framework of a collaborative project with 'Ice Age Journeys', Farndon Archaeological Research Investigations (FARI) and the Palaeolithic Archaeology research group from the University of Oxford. The 'Ice Age Journeys' project was previously supported by Heritage Lottery Funding. The authors from the British Geological Survey (BGS) were funded by BGS Teams 'Urban Geoscience' and 'Shallow Geohazards and Risks' and BGS Engineering Geology science programme. The authors are grateful to: Prof. N. Barton, Dr. S. Colcutt and W.G. Mills from Oxford University and Dr. Colin Baker for their collaboration; Dr. A.S. Howard, S. Price and Dr. S. Chenery from the BGS for the fruitful discussions during this research and all the volunteers involved during the archaeological excavations; and N. Ainiwaer for her help with the terrestrial laser scanning survey during a period of internship with the BGS. A. Myers from the BGS is greatly acknowledged for his invaluable help to create the supplementary materials of this paper. The BGS authors publish with the permission of the Executive Director of BGS, Natural Environment Research Council (NERC).

REFERENCES

Bailey, G. (2007) Time perspectives, palimpsests and the archaeology of time. Journal of Anthropological Archaeology 26 (2): 198–223. doi:10.1016/j.jaa.2006.08.002

Baker, C., Bateman, M., Bateman, P., Howard, J. (2013) The Aeolian sand record in the Trent Valley. Mercian Geologist 18 (2): 108–118.

Bateman, M.D. (1995) Thermoluminescence dating of the British coversand deposits. Quaternary Science Reviews 14 (7-8): 791–798. doi:10.1016/0277-3791(95)00053-4

Bateman, M.D. (1998) The origin and age of coversand in North Lincolnshire, UK. Permafrost Periglacial Processes 9: 313–325. doi:10.1002/(SICI)1099-1530(199810/12)9:4<313::AID-PPP297>3.0.CO;2-P

Brandon, A., Sumbler, M.G. (1988) An Ipswichian fluvial deposit at Fulbeck, Lincolnshire and the chronology of the Trent terraces. Journal of Quaternary Science 3: 127–133. doi: 10.1002/jqs.3390030204

721 Brandon, A., Sumbler, M.G. (1991) The Balderton Sand and Gravel: pre-Ipswichian cold stage fluvial
722 deposits near Lincoln, England. Journal of Quaternary Science 6 (2): 117–138. doi:
723 10.1002/jqs.3390060203
724 Bridgland, D.R, Howard, A.J., White, M.J., White, T.S. (2014) Quaternary of the Trent. Oxbow
725 Books, Oxford.
726 Brown, A.G., Carey, C. J., Howard, A. H., Challis, K.C., Cooper, L. (2005) Predictive modelling of
727 multiperiod geoarchaeological resources at a river confluence phase I. Unpublished report for
728 English Heritage, funded through the ALSF scheme. PNUM 3357.
729 Brown, A.G., Carey, C. J., Howard, A.H., Challis, K.C., Kincey, M. K., Tetlow, E., Cooper, L. (2007)
730 Predictive modelling of multiperiod geoarchaeological resources at a river confluence phase II.
731 Unpublished report for English Heritage, funded through the ALSF scheme. PNUM 3357.
732 BGS – British Geological Survey (1996) Nottingham sheet E126, solid and drift, 1:50,0000 series.
733 BGS – British Geological Survey (2016a) DiGMapGB-10. Last accessed on 16 June 2016 at
734 http://www.bgs.ac.uk/products/digitalmaps/DiGMapGB_10.html
735 BGS – British Geological Survey (2016b) Geology of Britain Viewer. Last accessed on 16 June 2016
736 at http://mapapps.bgs.ac.uk/geologyofbritain/home.html
737 BGS – British Geological Survey (2017) The BGS Lexicon of Named Rock Units.
738 http://www.bgs.ac.uk/lexicon/
739 Burton, D., Wood, L.J. (2010) Lidar Intensity as a Remote Sensor of Rock Properties. Search and
740 Discovery Article #40618. Last accessed on 12 August 2016 at
741 http://www.searchanddiscovery.com/pdfz/documents/2010/40618burton/ndx_burton.pdf.html
742 Challis, K. (2005) Airborne LiDAR: a tool for geoarchaeological prospection in Riverine landscapes.
743 In: H. Stoepker (Ed.), Archaeological Heritage Management in Riverine Landscapes, vol. 126
744 Rapportages Archeologische Monumentenzorg, Amersfoort, pp. 11–24.
745 Challis, K. (2006) Airborne laser altimetry in alluviated landscapes. Archaeological Prospection 13
746 (2): 103–127. doi: 10.1002/arp.272
747 Challis, K., Chris, C., Kincey, M., Howard, A.J. (2011) Assessing the preservation potential of
748 temperate, lowland alluvial sediments using airborne lidar intensity. Journal of Archaeological
749 Science 38 (2): 301–311. doi:10.1016/j.jas.2010.09.006
750 Clark C.D., Evans, D.J.A., Khatwa, A., Bradwell, T., Jordan, C.J., Marsh, S.H., Mitchell, W.A,
751 Bateman, M.D. (2004) Map and GIS database of glacial landforms and features related to the last
752 British Ice Sheet. Boreas 33: 359–375. doi:10.1111/j.1502-3885.2004.tb01246.x
753 Doneus, M., Neubauer, W. (2006) Laser scanners for 3D documentation of stratigraphic excavations.
754 In: Recording, Modeling and Visualization of Cultural Heritage, Baltsavias et al. (eds), Taylor &
755 Francis, pp. 193–203.

Doneus, M., Neubauer, W. (2005) 3D laser scanners on archaeological excavations. In: CIPA 2005 XX International Symposium, 26 September - 01 October 2005, Torino, Italy. Last accessed on 12 August 2016 at http://cipa.icomos.org/fileadmin/template/doc/TURIN/226.pdf

Edgeworth, M., deB Richter, D., Waters, C., Haff, P., Neal, C., Price, S.J. (2015) Diachronous beginnings of the Anthropocene: The lower bounding surface of anthropogenic deposits. The Anthropocene Review 2 (1): 33–58. doi:10.1177/2053019614565394

English Heritage (2012) Scheduling Selection Guide: Sites of Early Human Activity, p. 5. Last accessed on 12 August 2016 at https://historicengland.org.uk/images-books/publications/dssg-sites-early-human-activity/

English Heritage (2010) The Light Fantastic. Using airborne lidar in archaeological survey. English Heritage Publishing. Last accessed on 3 March 2017 at https://content.historicengland.org.uk/images-books/publications/light-fantastic/light-fantastic.pdf/

English Heritage (2011) 3D Laser Scanning for Heritage (second edition) Advice and guidance to users on laser scanning in archaeology and architecture. Last accessed on 3 March 2017 at http://content.historicengland.org.uk/images-books/publications/3d-laser-scanning-heritage2/3D_Laser_Scanning_final_low-res.pdf/

Fairburn, W.A., Bateman, M.D. (2016) A new multi-stage recession model for Proglacial Lake Humber during the retreat of the last British–Irish Ice Sheet. Boreas 45: 133–151. doi: 10.1111/bor.12140

Fisher, E.C., Akkaynak, D., Harris, J., Herries, A.I.R., Jacobs, Z., Karkanas, P., Marean, C.W., McGrath, J.R. (2015) Technical considerations and methodology for creating high-resolution, color-corrected, and georectified photomosaics of stratigraphic sections at archaeological sites. Journal of Archaeological Science 57: 380–394. doi:10.1016/j.jas.2015.02.022

Folk, R.L. (1974) Petrology of Sedimentary Rocks. Hemphill, Austin, TX, p. 184

Garton, D. (1993) A Late Upper Paleolithic site near Newark, Nottinghamshire. Transactions of the Thoroton Society of Nottinghamshire 97: 144.

Garton, D., Jacobi, R.M. (2009) An extensive Late Upper Palaeolithic flint scatter at Farndon Fields, near Newark, Nottinghamshire. Archaeological Journal 166: 1–37. doi: 10.1080/00665983.2009.11078219

Garton, D., Baker, C., Banks, V., Barton, N., Budge, D., Collcutt, S., Price, S., Ross, I., Tapete, D., Tyndall, R. (2015) Ice Age Journeys: research by a community archaeology group at Farndon Fields, Nottinghamshire. Transactions of the Thoroton Society of Nottinghamshire 119: 103-140.

Harding, P., Ellis, C., Grant, M.J. (2014) Late Upper Palaeolithic Farndon Fields. In: Cooke, Nicholas and Mudd, Andrew (eds.) A46 Nottinghamshire: The Archaeology of the Newark to Widmerpool Improvement Scheme, 2009. Salisbury, GB, Wessex Archaeology, pp. 12-70.

Highways Agency (2012) Following the Fosse Way through Nottinghamshire. Archaeology and the A46. Cotswold Wessex Archaeology, 16 pp. Last accessed on 12 August 2016 at http://assets.highways.gov.uk/roads/road-projects/a46-newark-to-widmerpool-improvement/m120008_Following_the_Fosse_Way_through_Nottinghamshire_Archaeology_and_the_A46_proof_low.pdf

Howard, A.S., Warrington, G., Carney, J.N., Ambrose, K., Young, S.R., Pharaoh, T.C., Cheney, C.S. (2009) Geology of the Nottingham District. Memoir of the British Geological Survey, Sheet 126 (England and Wales).

Howard, A.J., Bridgland, D.R., Knight, D., McNabb, J., Rose, J., Schreve, D.C., Westaway, R., White, M.J., White, T.S. (2007) The British Pleistocene fluvial archive: East Midlands drainage evolution and human occupation in the context of the British and NW European record. Quaternary Science Reviews 26 (22-24): 2724–2737. doi:10.1016/j.quascirev.2007.06.029

Howard, A.J., Brown, A.G., Carey, C.J., Challis, K., Cooper, L.P., Kincey, M., Toms, P. (2008) Archaeological resource modelling in temperate river valleys: a case study from the Trent Valley, UK. Antiquity, 82(318): 1040–1054. doi: 10.1017/S0003598X00097763

Howard, A.J., Carney, J.N., Greenwood, M.T., Keen, D.H., Mighall, T., O'Brien, C., Tetlow, E. (2011) The Holme Pierrepont sand and gravel and the timing of Middle and Late Devensian floodplain aggradation in the English Midlands. Proceedings of the Geologists' Association 122(3): 419–431. doi:10.1016/j.pgeola.2011.03.009

Jacobi, R.M., Higham, T.F.G. (2009). The early Lateglacial re-colonization of Britain: new radiocarbon evidence from Gough's Cave, southwest England. Quaternary Science Reviews 28: 1895–1913. doi:10.1016/j.quascirev.2009.03.006

Kinsley, G., Knight, D. (1992) Archaeology of the Fosse Way. Vol. 2: Newark to Widmerpool. Trent & Peak Archaeological Trust.

Knight, D. (2004) A46 Newark to Widmerpool Improvement: archaeological research framework. Report for Highways Agency, 22.11.04, Trent & Peak Archaeological Unit, p. 8.

Knight, D., Howard, A.J. (2004) Trent Valley Landscapes. The Archaeology of 500 000 years of change. Trent Valley Geoarchaeology. Heritage Marketing and Publications Limited, 202 pp.

Knight, D., Vyner, B., Allen, C. (2012) East Midlands Heritage. An Updated Research Agenda and Strategy for the Historic Environment of the East Midlands. Nottingham Archaeological Monographs 6, Buxton Press, Buxton, Derbyshire, p. 29.

Koster, E.A. (1988) Ancient and modern cold-climate aeolian sand deposition: a review. Journal of Quaternary Science 3 (1): 69-83. doi: 10.1002/jqs.3390030109

Krooks, A., Kaasalainen, S., Hakala, T., Nevalainen, O. (2013) Correction of intensity incidence angle effect in terrestrial laser scanning. In: ISPRS Annals of the Photogrammetry, Remote Sensing and

826 Spatial Information Sciences, Volume II-5/W2, 2013 ISPRS Workshop Laser Scanning 2013, 11 –
827 13 November 2013, Antalya, Turkey, pp. 145-150. Accessed at http://www.isprs-ann-photogramm-
828 remote-sens-spatial-inf-sci.net/II-5-W2/145/2013/isprsannals-II-5-W2-145-2013.pdf
829 Lerma, J.L., Navarro, S., Seguí, A.E., Cabrelles, M. (2014) Range-based versus automated markerless
830 image-based techniques for rock art documentation. Photogrammetric Record 29 (145): 30–48. doi:
831 10.1111/phor.12054
832 Malone, S.J. (2012) Lincolnshire Fenland Lidar. Heritage Trust. Working Paper 1. Lincolnshire/
833 Archaeology Project Services. British Archaeology 127: 48–49.
834 Pfeifer, N., Dorninger, P., Haring, A., Fan, H. (2007) Investigating terrestrial laser scanning intensity
835 data: quality and functional relations, pp. 328-337 Last accessed on 12 August 2016 at
836 http://publik.tuwien.ac.at/files/pub-geo_1932.pdf
837 Price, D., Rogers, P.J. (1978) The sand and gravel resources of the country west of Newark on Trent,
838 Nottinghamshire. Description of 1: 25 000 resource sheet SK 75. Mineral Assessment Report
839 Institute Geological Sciences, 31, 70 pp.
840 Rapp, G.R., Hill, C.L. (2006). Geoarchaeology: The Earth-Science Approach to Archaeological
841 Interpretation. New Haven; London: Yale University Press.
842 Sanger, M.C. (2005) Determining depositional events within shell deposits using computer vision and
843 photogrammetry. Journal of Archaeological Science 53: 482–491. doi:10.1016/j.jas.2014.10.026
844 Schiffer, M.B. (1987) Formation processes of the archaeological record. Albuquerque, NM: University
845 of New Mexico Press.
846 TPAU – Trent and Peak Archaeology Unit (2004) Trent and Peak Archaeological Unit (2004) Farndon
847 Fields, Nottighamshire: Assessment of the Evidence for the Late Upper Palaeolithic Activity and Its
848 Importance. Unpublished client report ref FNW 2.
849 Vandenberghe, J. (2013) Cryoturbation Structures. In: Encyclopedia of Quaternary Science, vol. 3, pp.
850 430-435, revision of the previous edition article Vandenberghe, J. (2007) Periglacial landforms.
851 Cryoturbation Structures. In: Encyclopedia of Quaternary Science, S.A. Elias (ed), Elsevier,
852 Oxford, 2007, pp. 2147-2153. Last accessed on 12 August 2016 at
853 https://www.researchgate.net/publication/282677513_Cryoturbation_structures
854 Wessex Archaeology (1995) Farndon Fields, Newark on Trent, Nottinghamshire. Archaeological
855 Evaluation. Fieldwalking, Auger Survey and test pitting.
856 Wessex Archaeology (2006) Newark to Widmerpool Improvements Archaeological Works at Farndon
857 Fields (A46 FAR05) Fieldwork Report. 29 pp.